The Calorimeter Response Function

Response = Average signal per unit of deposited energy

e.g. # photoelectrons/GeV, picoCoulombs/MeV, *etc.*

➡ A *linear* calorimeter has a *constant response*

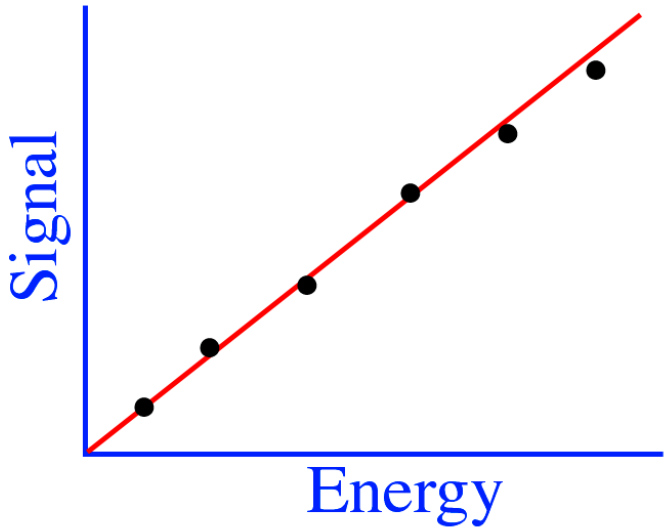

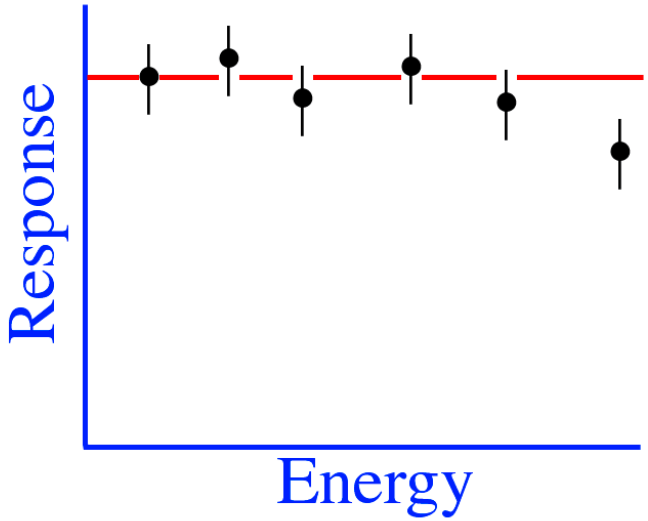

Electromagnetic calorimeters are in general *linear*

All energy deposited through ionization/excitation of absorber

If *not* linear → instrumental effect (saturation, leakage,.....)

Signal linearity for electromagnetic showers

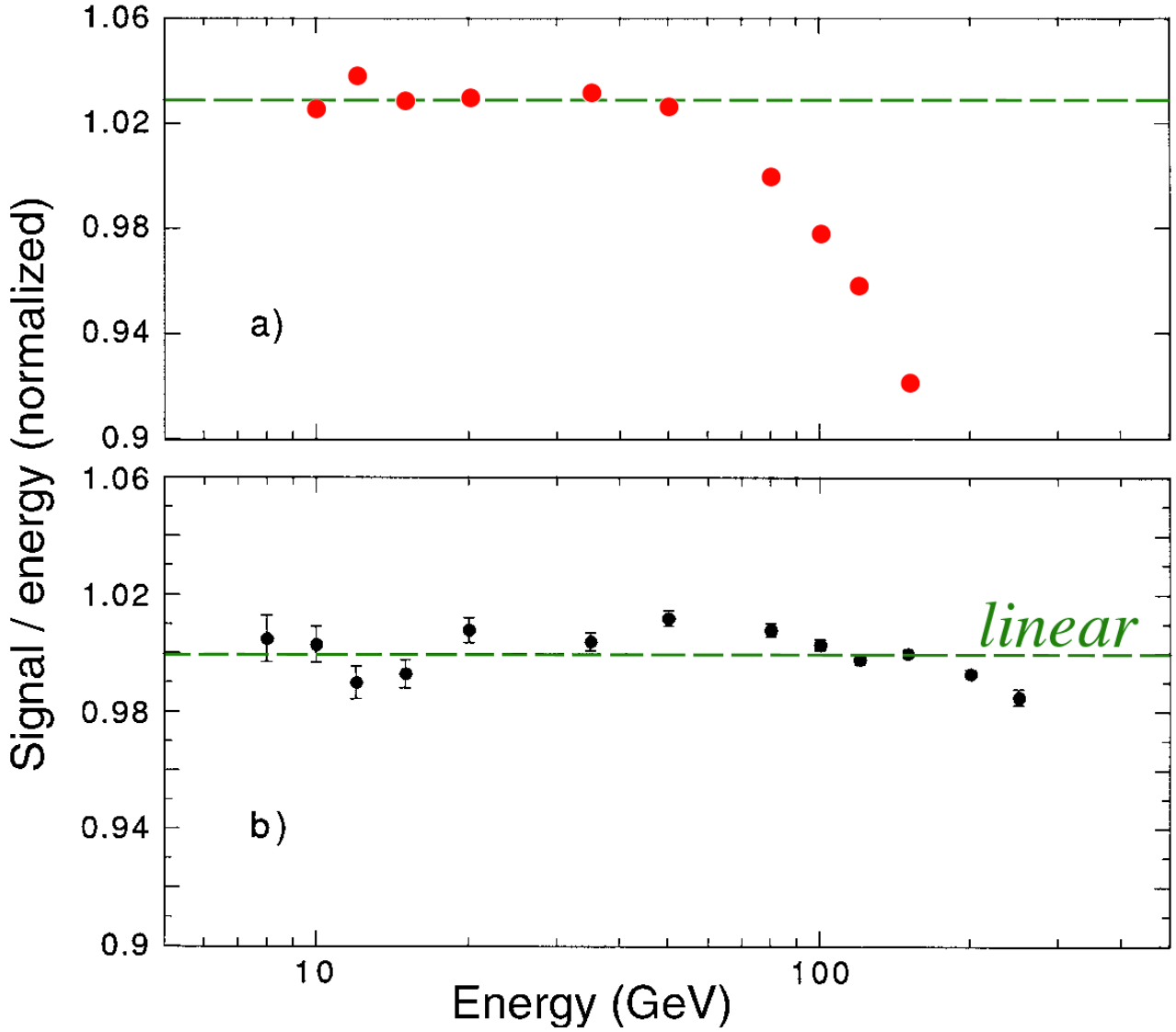

FIG. 3.1. The em calorimeter response as a function of energy, measured with the QFCAL calorimeter, before (a) and after (b) precautions were taken against PMT saturation effects. Data from [Akc 97].

Fluctuations due to instrumental effects (readout)

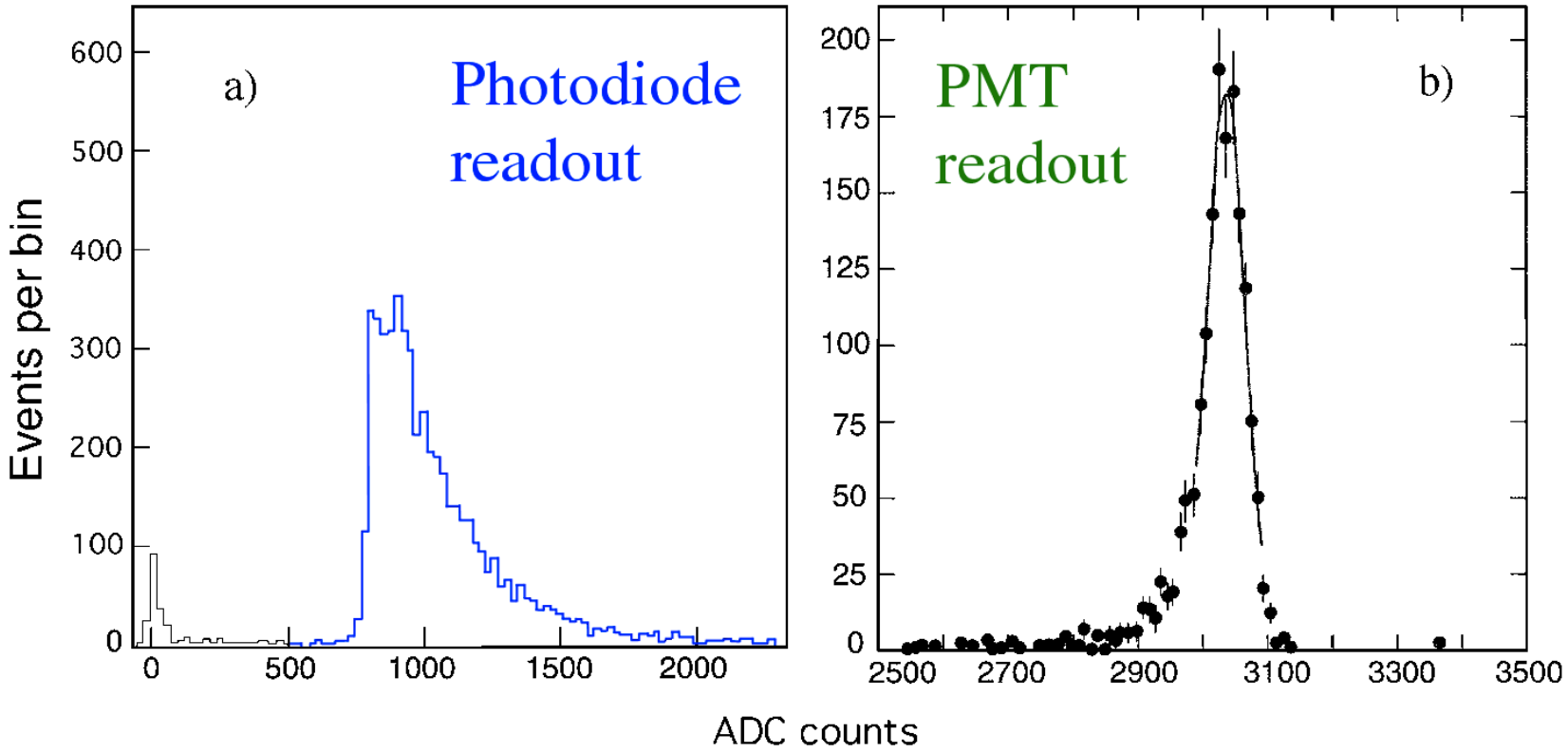

FIG. 3.3. Signal distributions for high-energy electron showers measured with a prototype $PbWO_4$ crystal calorimeter. The calorimeter was read out either with silicon photodiodes (a) or with photomultiplier tubes (b). Data from [Pei 96].

Sampling

- There are *homogeneous* and *sampling* calorimeters
  - Homogeneous: Absorber and active medium are the same
  - Sampling: Only part of shower energy deposited in active medium

$$\textit{Sampling fraction}\ (f_{\text{samp}}) = \frac{\text{energy deposited in active medium}}{\text{total energy deposited in calorimeter}}$$

- f_{samp} is usually determined with a *mip* (dE/dx minimum)

  N.B. *mip*'s do not exist!

  e.g. D0 (em section):

  $3\,\text{mm}\ {}^{238}\text{U}$ $\quad (dE/dx = 61.5\ \text{MeV/layer})$

  $2 \times 2.3\,\text{mm}\ \text{LAr}$ $\quad (dE/dx = 9.8\ \text{MeV/layer})$

  $\Big\}\rightarrow f_{\text{samp}} = 13.7\%$

The *e/mip* ratio

- D0: $f_{\text{samp}} = 13.7\%$
  However, for em showers, sampling faction is only 8.2%
  ➡ *e/mip* ≈ 0.6

- *e/mip* is a function of *shower depth*, in U/Lar it *decreases*
  e/mip increases when the *sampling frequency* becomes very high
  What is going on?

- *Photoelectric effect:* $\sigma \propto Z^5$, $(18/92)^5 = 3 \cdot 10^{-4}$
  $\rightarrow$ Soft γs are very inefficiently sampled
  Effects strongest at high Z, and late in the shower development
  The range of the photoelectrons is typically < 1 mm
  $\rightarrow$ if absorber layers are thin, they may contribute to the signals

Sampling calorimeters: The e/mip signal ratio

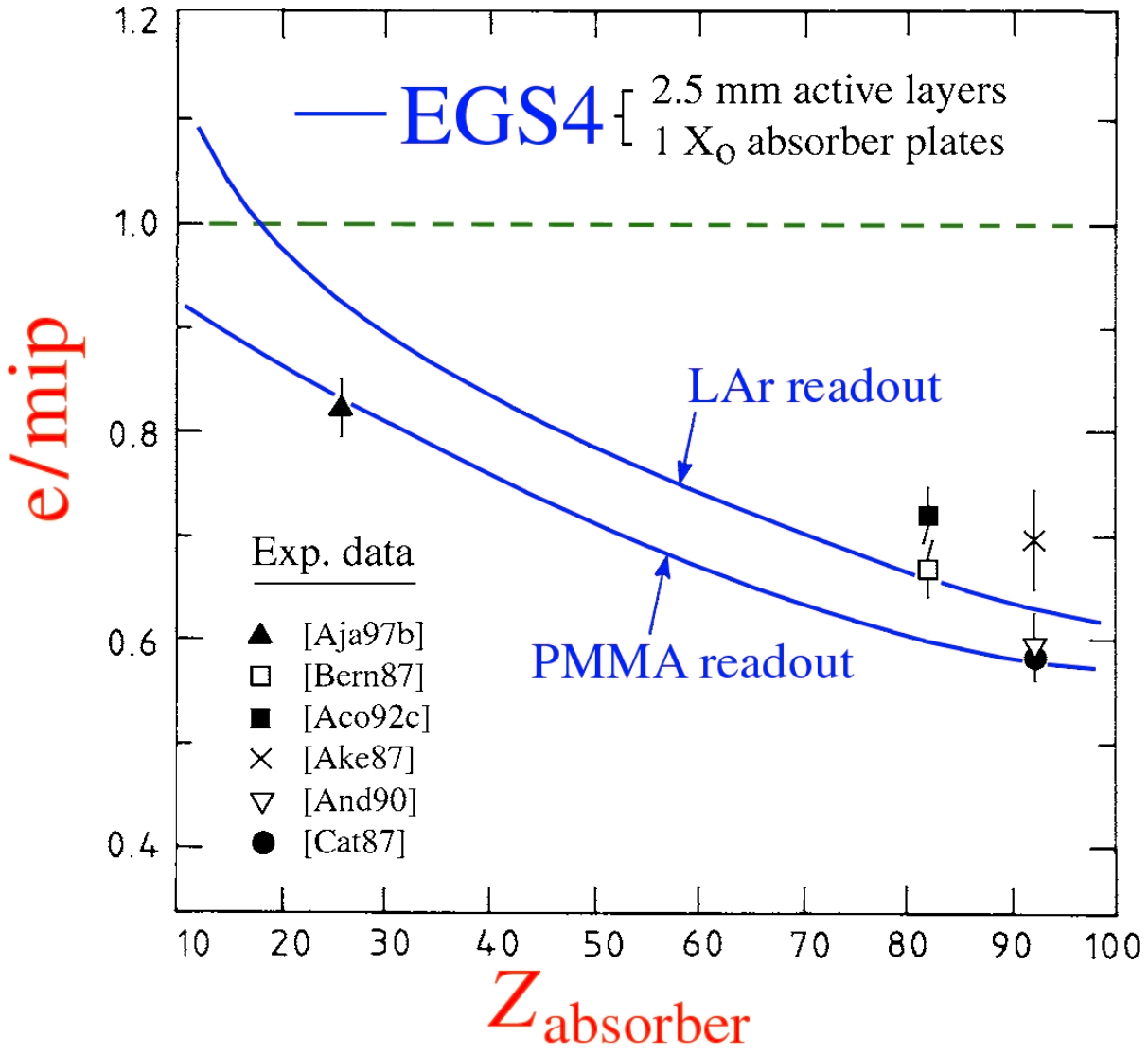

FIG. 3.7. The e/mip ratio for sampling calorimeters as a function of the Z value of the absorber material, for calorimeters with plastic scintillator or liquid argon as active material. Experimental data are compared with results of EGS4 Monte Carlo simulations [Wig 87].

The EM sampling fraction changes with depth!

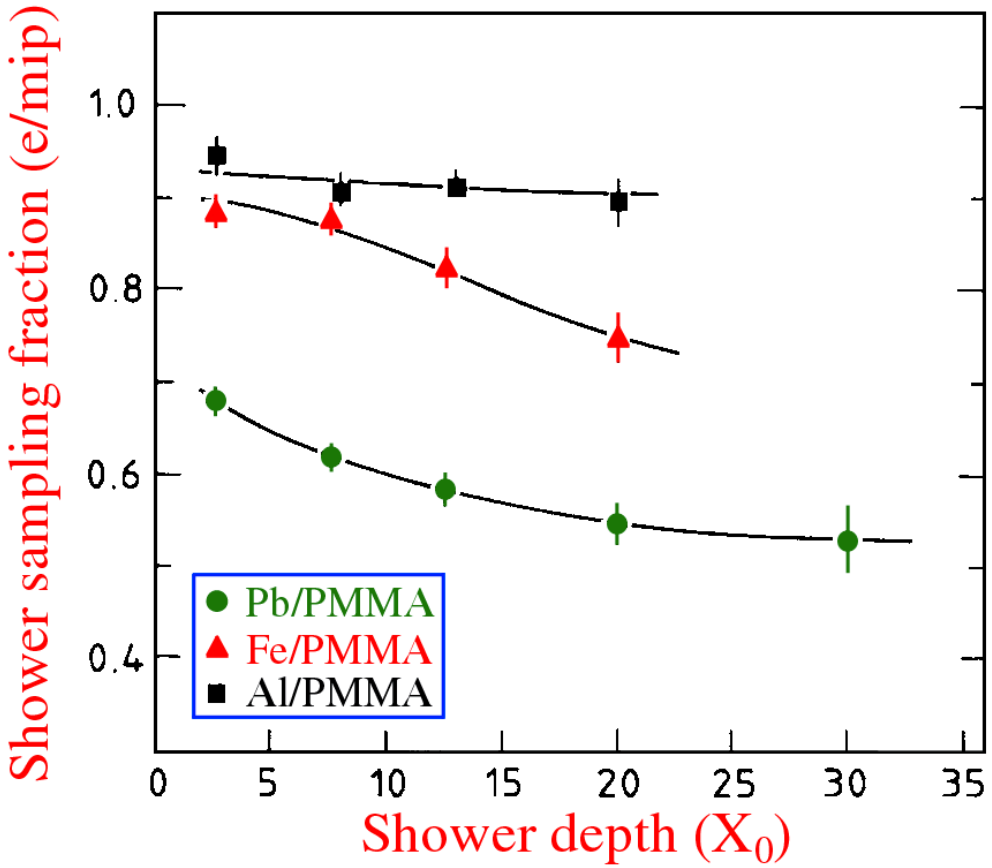

FIG. 3.8. The e/mip ratio as a function of the shower depth, or age, for 1 GeV electrons in various sampling calorimeter configurations. All calorimeters consist of 1 X_0 thick absorber layers, interleaved with 2.5 mm thick PMMA layers. Results from EGS4 Monte Carlo simulations [Wig 87].

The e/mip ratio: Dependence on calorimeter parameters

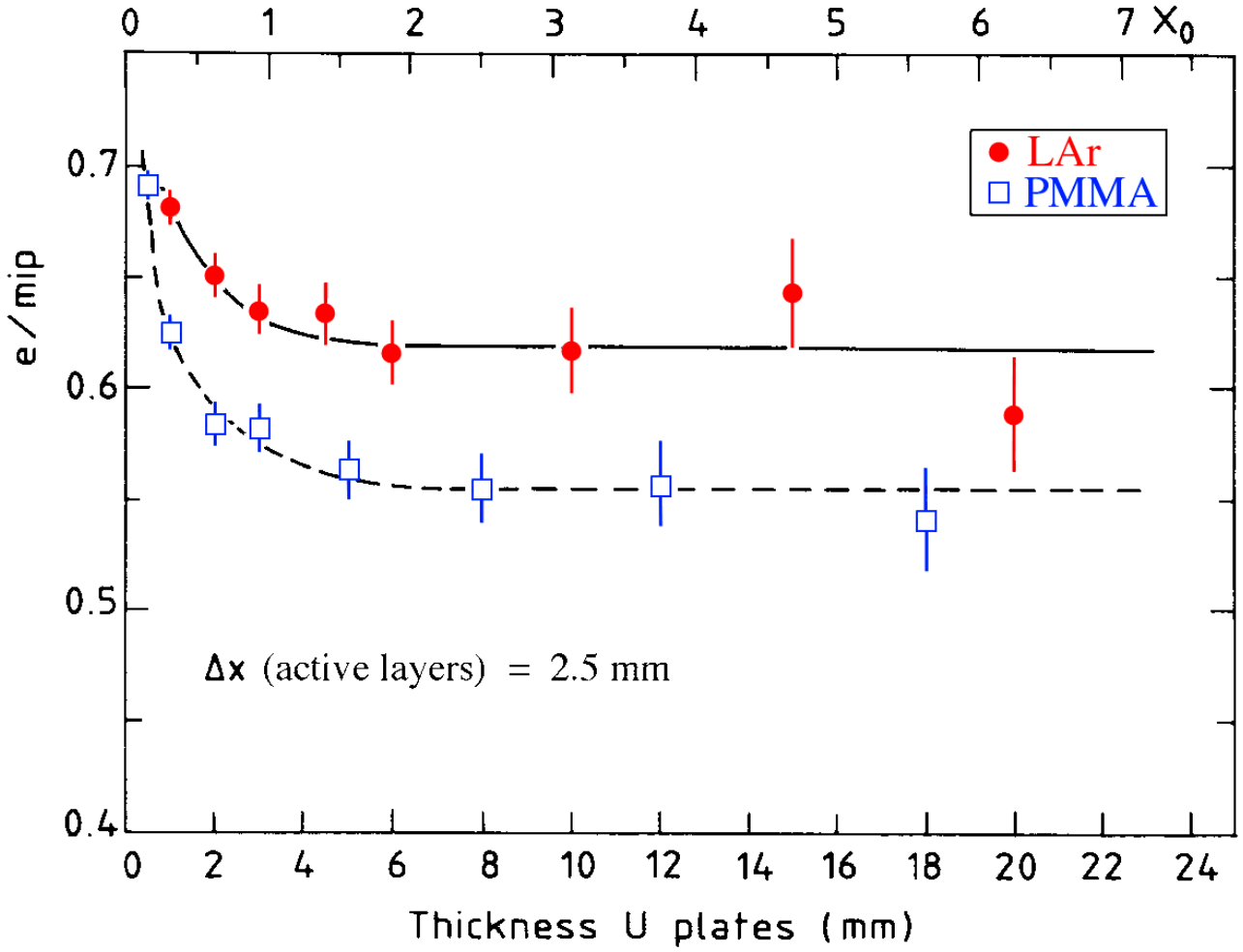

FIG. 3.9. The e/mip ratio as a function of the thickness of the absorber layers, for uranium/PMMA and uranium/LAr calorimeters. The thickness of the active layers is 2.5 mm in all cases. Results from EGS4 Monte Carlo simulations [Wig 87].

Hadronic shower response and the *e/h* ratio

- *The hadronic response is* ***not constant***

  $f_{\rm em}$, and therefore e/π signal ratio is a function of energy

  ➡ If calorimeter is linear for electrons, it is *non-linear* for hadrons

- Energy-independent way to characterize hadron calorimeters: *e/h*

  e = response to the em shower component

  h = response to the non-em shower component

  → Response to showers initiated by pions:

$$R_\pi = f_{\rm em}\, e \;+\; \big[1 - f_{\rm em}\big] h \quad \rightarrow \quad \boxed{e/\pi = \frac{e/h}{1 - f_{\rm em}\big[1 - e/h\big]}}$$

  e/h is inferred from e/π measured at several energies ($f_{\rm em}$ values)

- Calorimeters can be

  Undercompensating $(e/h > 1)$

  Overcompensating $(e/h < 1)$

  Compensating (e/h = 1)

Hadron showers: e/h and the e/π signal ratio

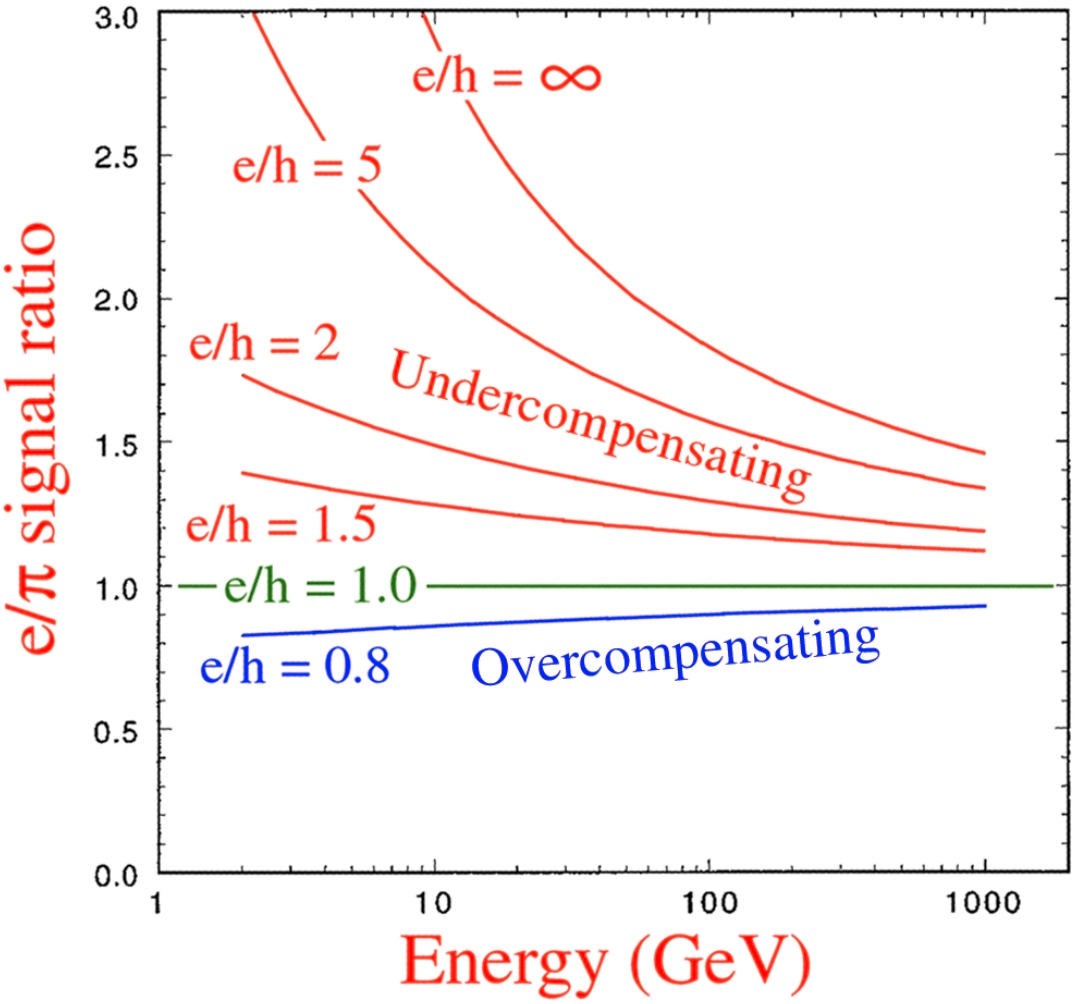

FIG. 3.4. The relation between the calorimeter response ratio to em and non-em energy deposition, e/h, and the measured e/π signal ratios. See text for details.

Hadronic signal (non-)linearity: Dependence on e/h

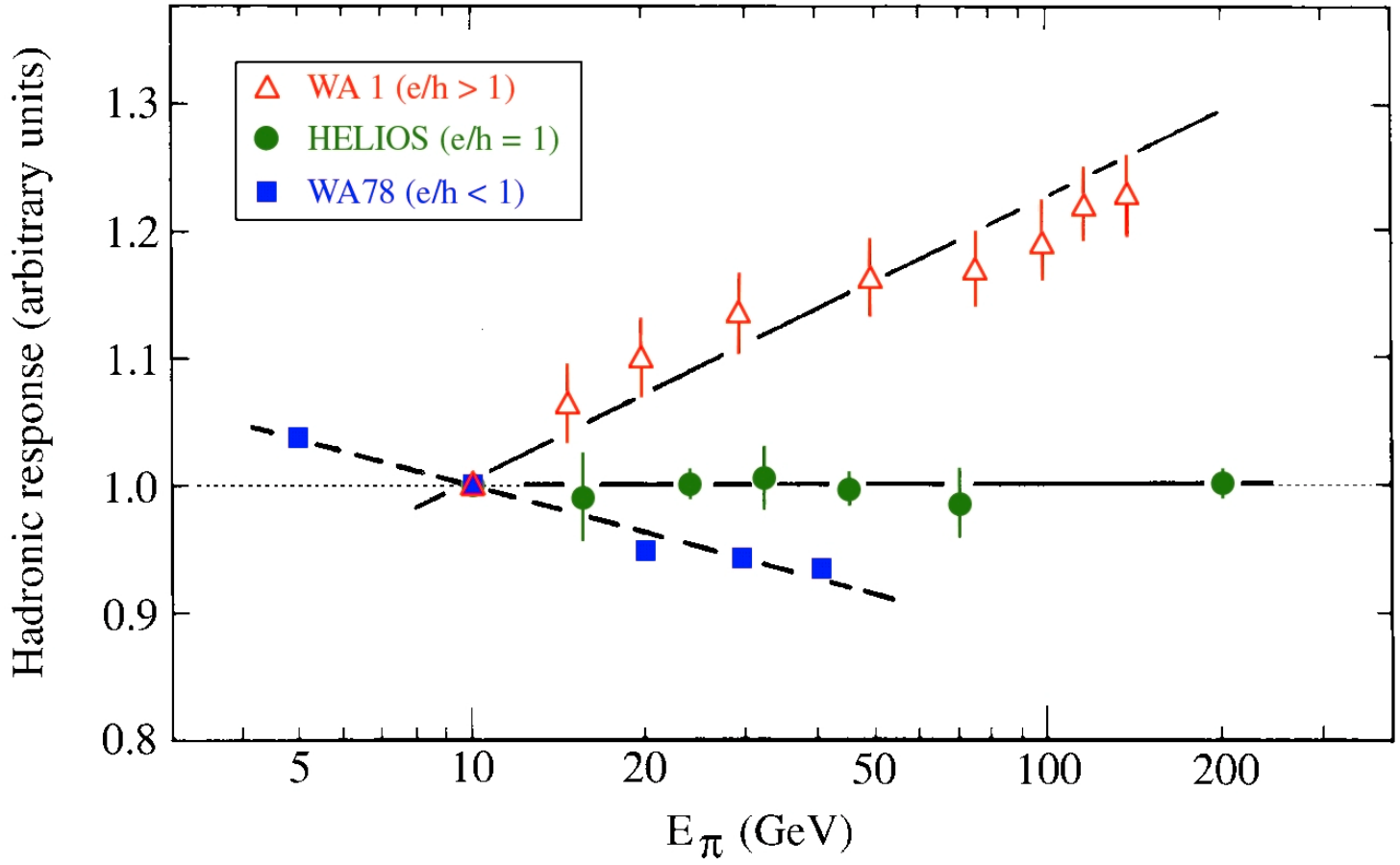

FIG. 3.14. The response to pions as a function of energy for three calorimeters with different e/h values: the WA1 calorimeter ($e/h > 1$, [Abr 81]), the HELIOS calorimeter ($e/h \approx 1$, [Ake 87]) and the WA78 calorimeter ($e/h < 1$, [Dev 86, Cat 87]). All data are normalized to the results for 10 GeV.

Compensation (1)

Need to understand response to typical shower particles (relative to *mip*)

Spallation protons and *Neutrons*

- *Spallation protons*

  More efficient sampling

  Signal saturation

Aspects of compensation: Sampling of soft shower protons

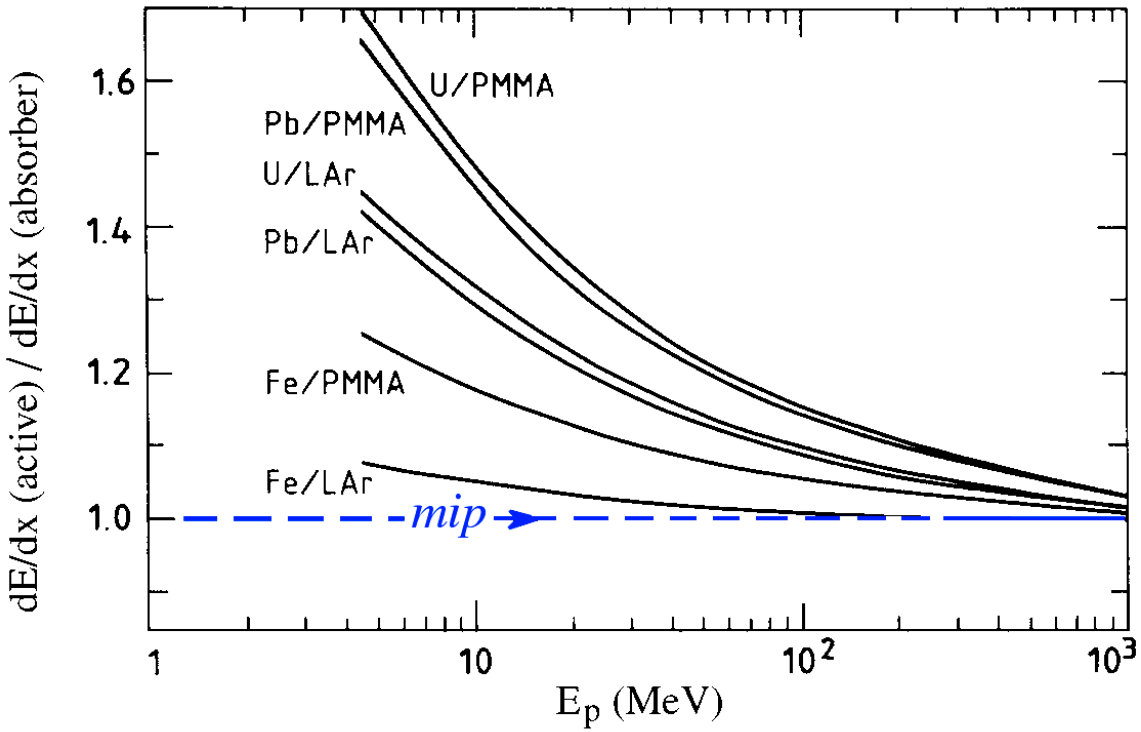

FIG. 3.15. The ratio of energy deposition by non-relativistic protons in the active and passive materials of various calorimeter structures, as a function of the proton s kinetic energy. This ratio is normalized to the one for mips. From [Wig 87].

Aspects of compensation: Saturation effects

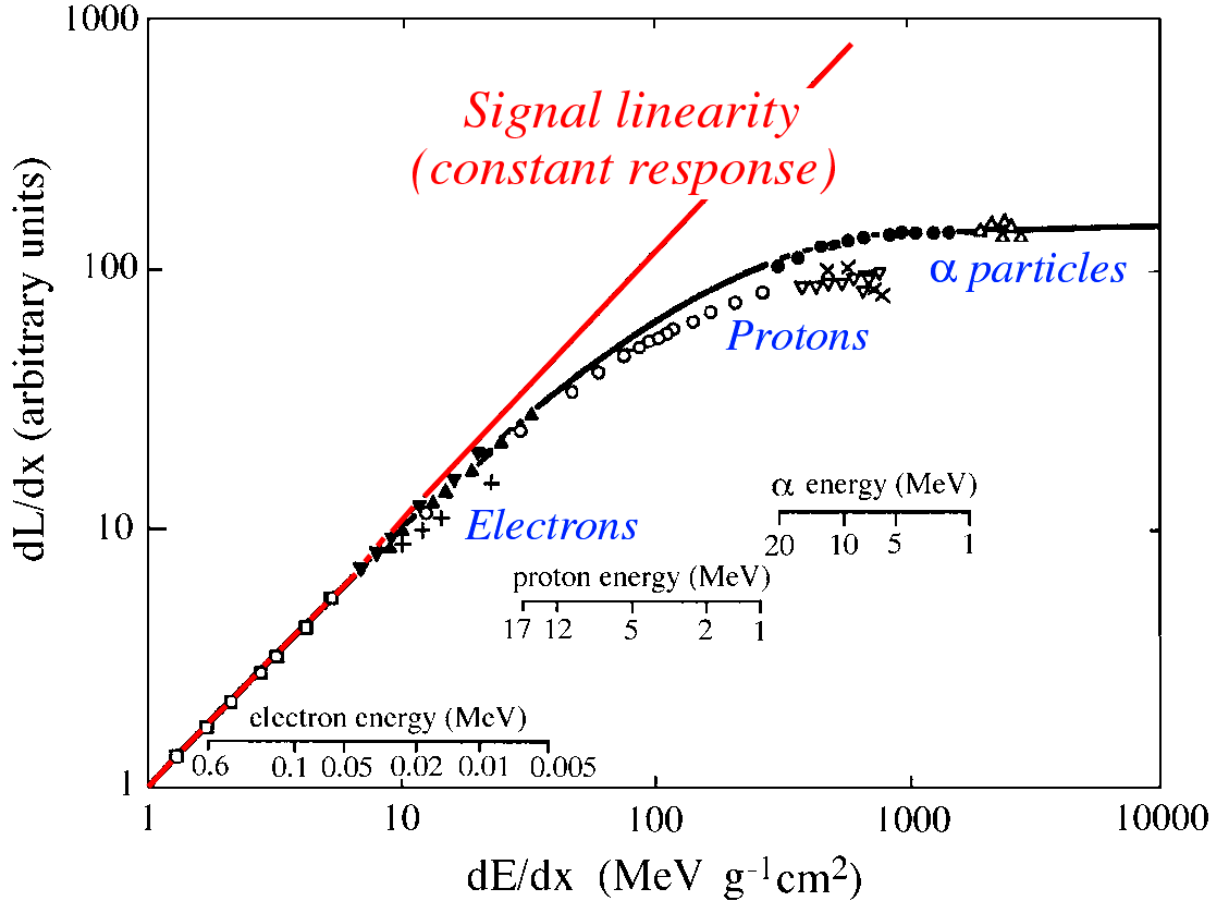

FIG. 3.25. Variation of the specific fluorescence, dL/dx, with the specific ionization loss, dE/dx, in anthracene crystals. The solid curve represents Equation 3.13 with $k_B = 6.6$ mg cm^{-2} MeV^{-1}.

Compensation: The spallation proton/mip signal ratio

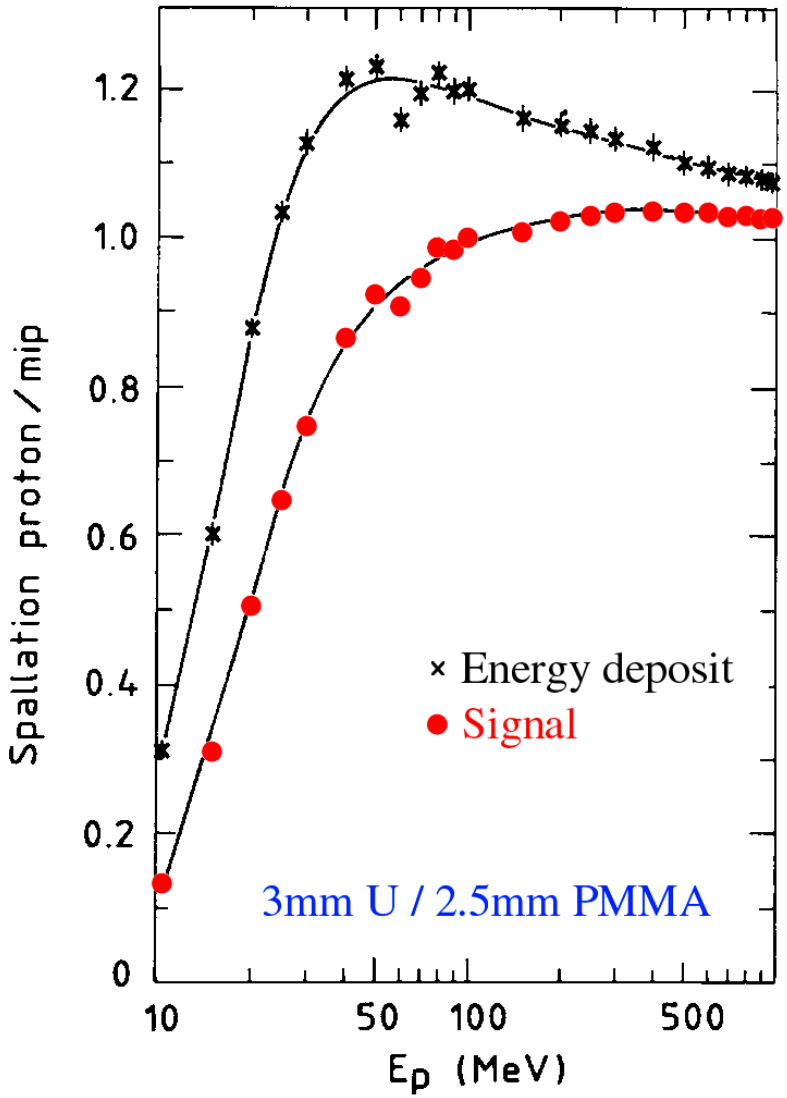

FIG. 3.16. The energy deposit in the active layers (upper curve) and the calorimeter signal (lower curve) for stopping protons, relative to mips, as a function of the kinetic proton energy, in a 3 mm U/2.5 mm PMMA sampling calorimeter. See text for details. Results from Monte Carlo simulations [Wig 87].

Compensation (2)

Need to understand response to typical shower particles (relative to *mip*)

Spallation protons and *Neutrons*

- *Neutrons*
  - $(n, n'\gamma)$ *inelastic* scattering: not very important
  - (n, n') *elastic* scattering: most interesting ⟵
  - (n, γ) *capture* (thermal): lots of energy, but process is slow (μs)

Compensation (3) – The role of neutrons

- *Elastic scattering* $f_{\text{elastic}} = 2A/(A+1)^2$

  Hydrogen $f_{\text{elastic}} = 0.5$, Lead $f_{\text{elastic}} = 0.005$

  Pb/H_2 calorimeter structure (50/50)

  1 MeV n deposits 98.3% in H_2
  mip deposits 2.2% in H_2
  $\Big\}\!\!\rightarrow$ *n/mip = 45*

- *Recoil protons can be measured!*

  ➡ Neutrons have an enormous potential to amplify hadronic shower signals, and thus *compensate* for losses in invisible energy

- *Tune the e/h value through the sampling fraction!*

  e.g. 90% Pb/10% H_2 calorimeter structure

  1 MeV n deposits 86.6% in H_2
  mip deposits 0.25% in H_2
  $\Big\}\!\!\rightarrow$ *n/mip = 350*

Compensation: The importance of soft neutrons

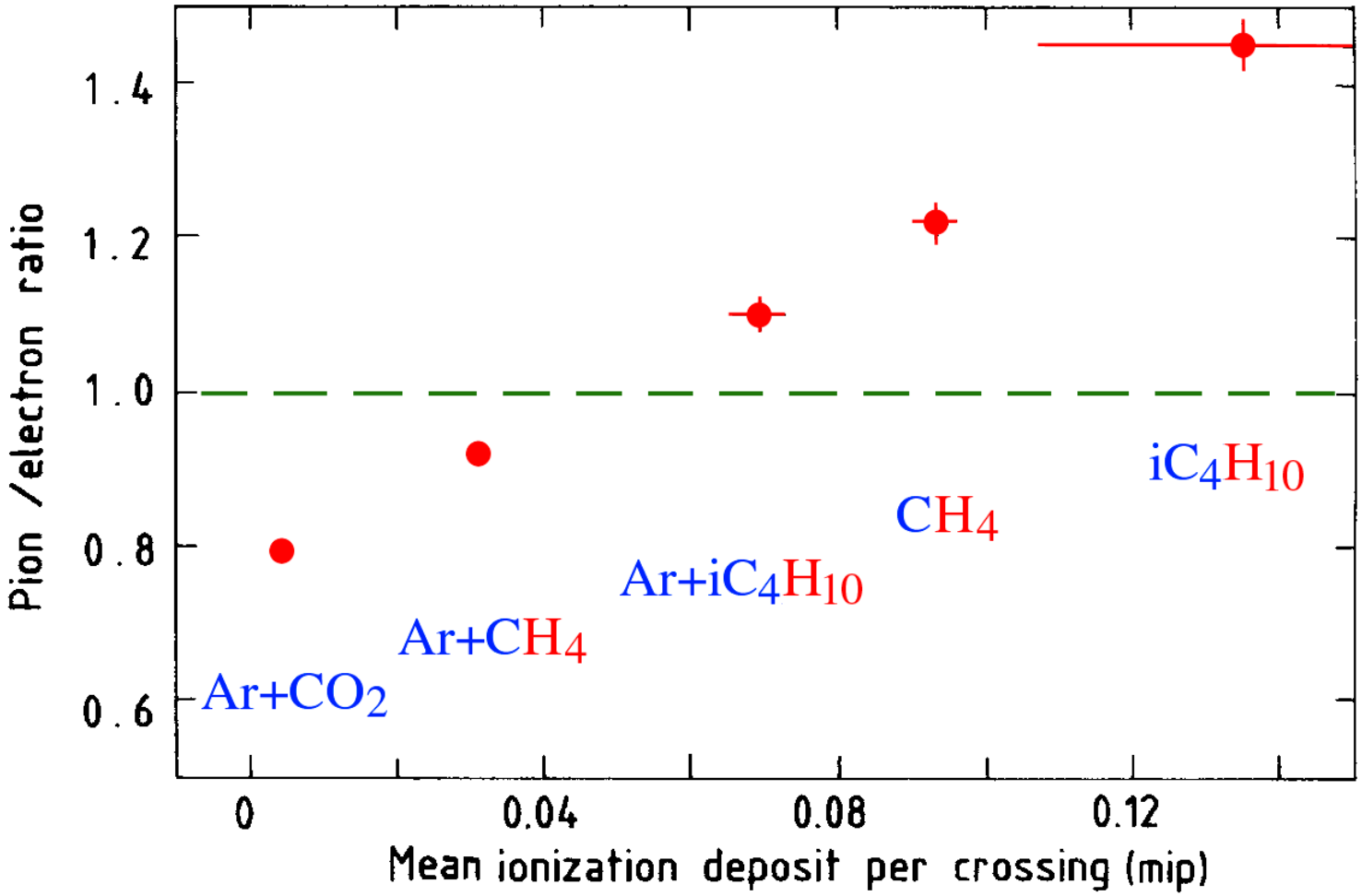

FIG. 3.32. The pion/electron signal ratio, averaged over the energy range 1 5 GeV, measured for different gas mixtures with the uranium/gas calorimeter of the L3 Collaboration. The horizontal scale gives the (calculated) average energy deposit in a chamber gap by slow neutrons [Gal 86].

Compensation: The crucial role of the sampling fraction

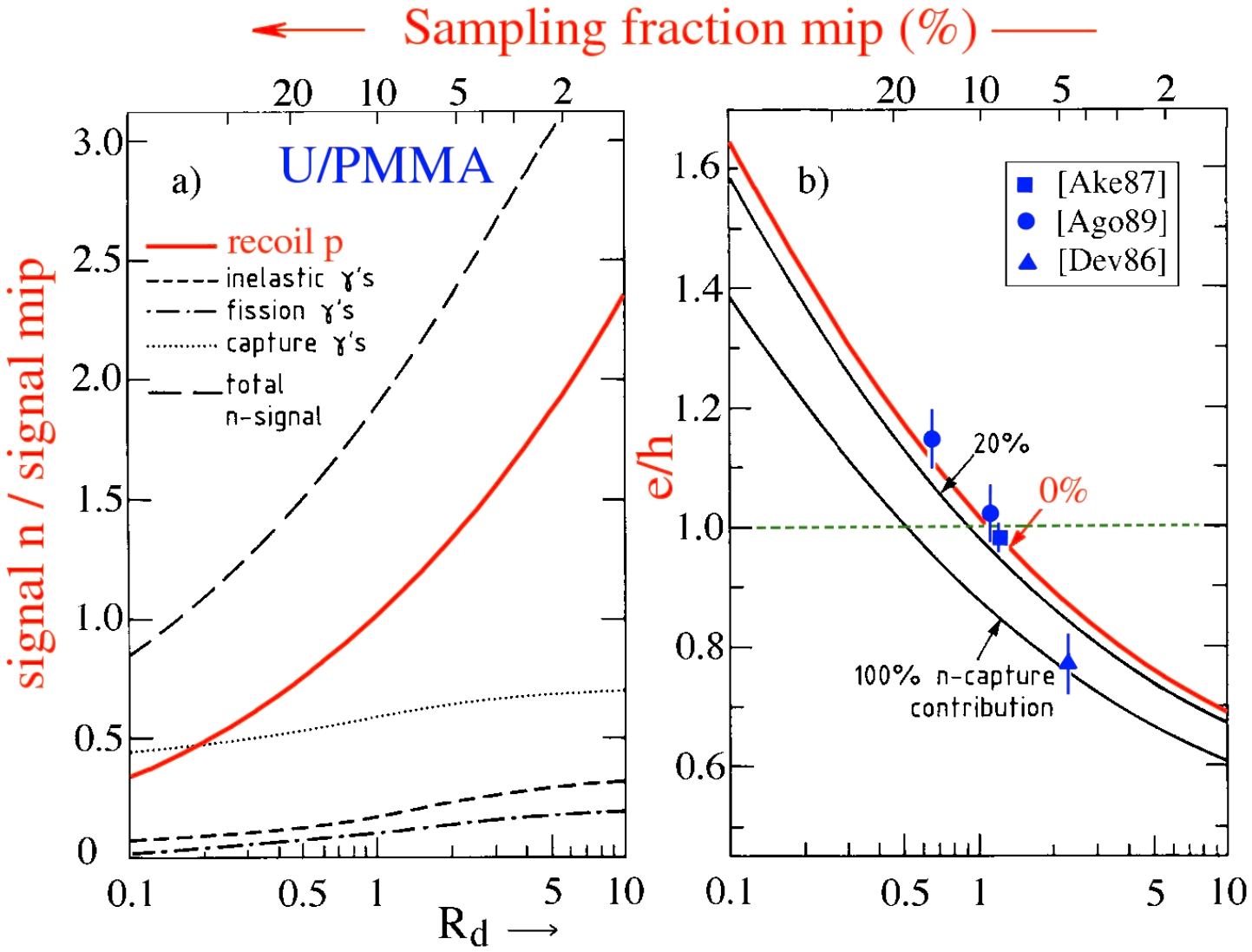

FIG. 3.33. The n/mip response ratio, split up into its components, for ^{238}U/PMMA calorimeters, as a function of R_d, the ratio of the thicknesses of the passive and active calorimeter layers (a). The e/h ratio as a function of R_d, assuming that 0%, 20% or 100% of the γs released in thermal neutron capture contribute to the calorimeter signals (b). The top axis of both graphs indicates the sampling fraction for mips. From [Wig 88].

Compensation in practice: Pb/scintillator calorimeters

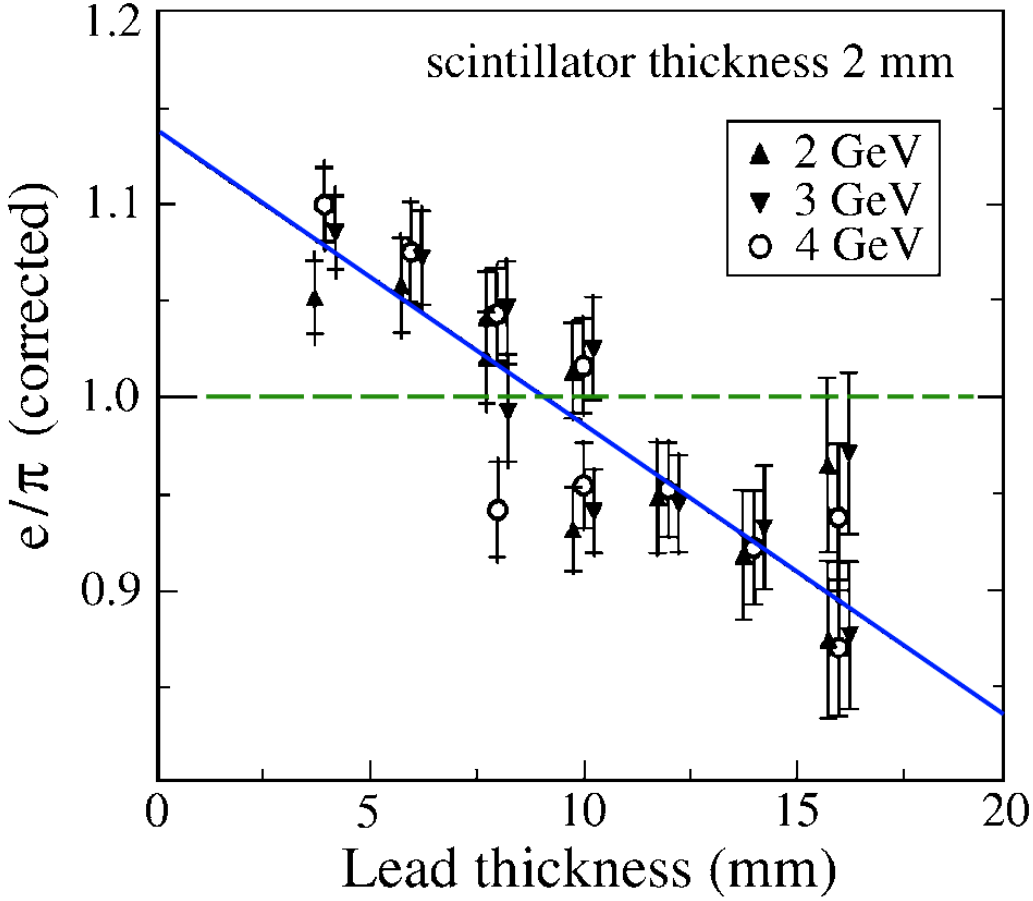

FIG. 3.35. The e/π signal ratio, corrected for the effects of shower leakage, for lead/polystyrene-scintillator calorimeters, as a function of the thickness of the lead plates, for 2 mm thick scintillator plates. The inner (outer) error bars show the combined systematic and statistical uncertainty without (with) the shower leakage corrections. The line in the plot is a result of a linear fit to the experimental data [Suz 99].

Compensation in Fe/scintillator calorimeters?

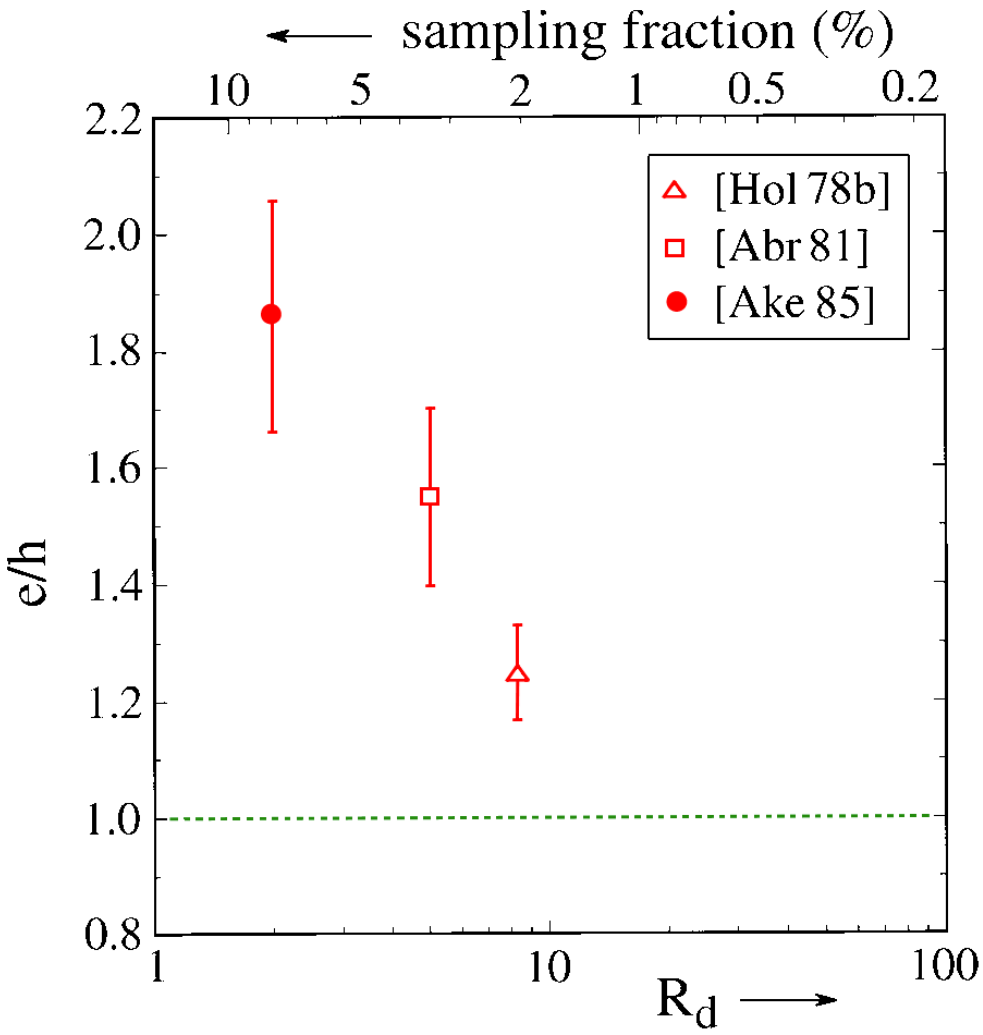

FIG. 3.36. The e/h value for iron/plastic-scintillator calorimeters, as a function of the sampling fraction for mips (top horizontal scale), or the volume ratio of the amounts of passive and active material (bottom horizontal scale).

Compensation: Slow neutrons and the signal's time structure

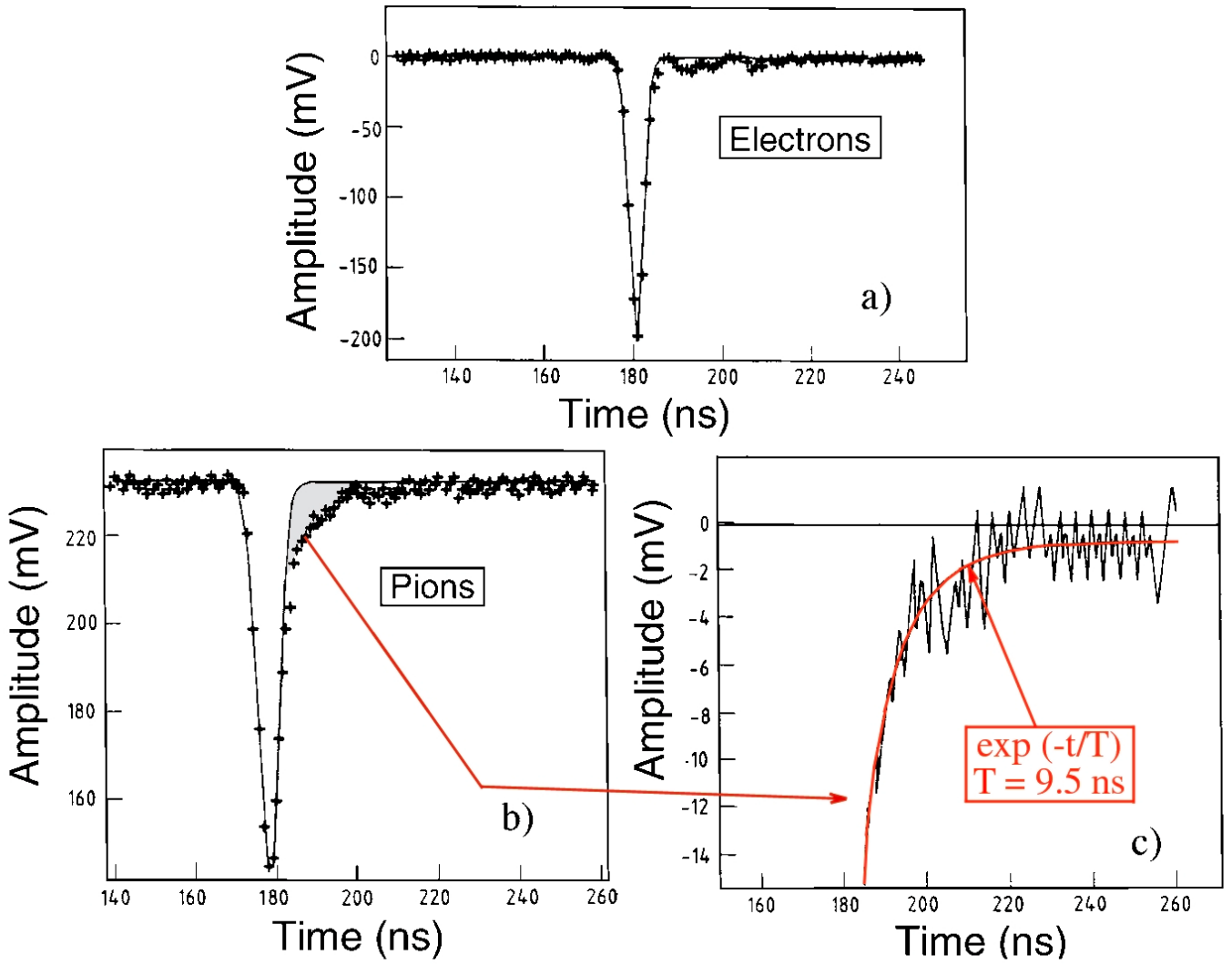

FIG. 3.24. Typical calorimeter signals for 150 GeV electrons (a) and pions (b) measured with the SPACAL calorimeter. The pion signal exhibits a clear exponential tail with a time constant of $\sim$ 10 ns (c). The $t = 0$ point is arbitrary and the bin size is 1 ns. Data from [Aco 91a].

Non-hydrogenous calorimeters: Z dependence of e/h

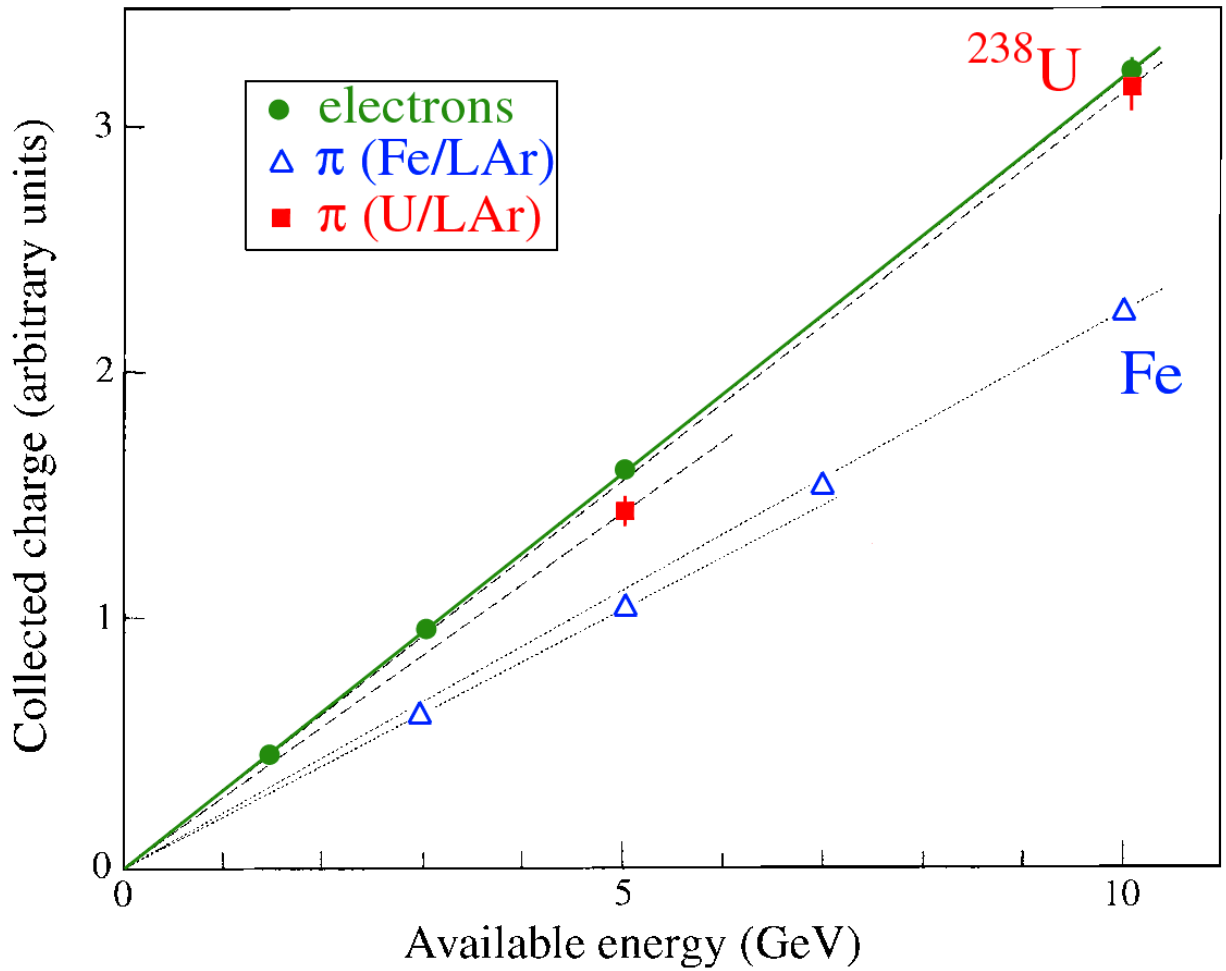

FIG. 3.28. The average charge collected from hadrons and electrons, as a function of energy, in liquid-argon calorimeters with iron or depleted uranium as absorber material. The charge is measured in arbitrary units, which are different for the two calorimeters, but which result in the same response for electrons. Data from [Fab 77].

Compensation: Effect of slow neutrons on the signals

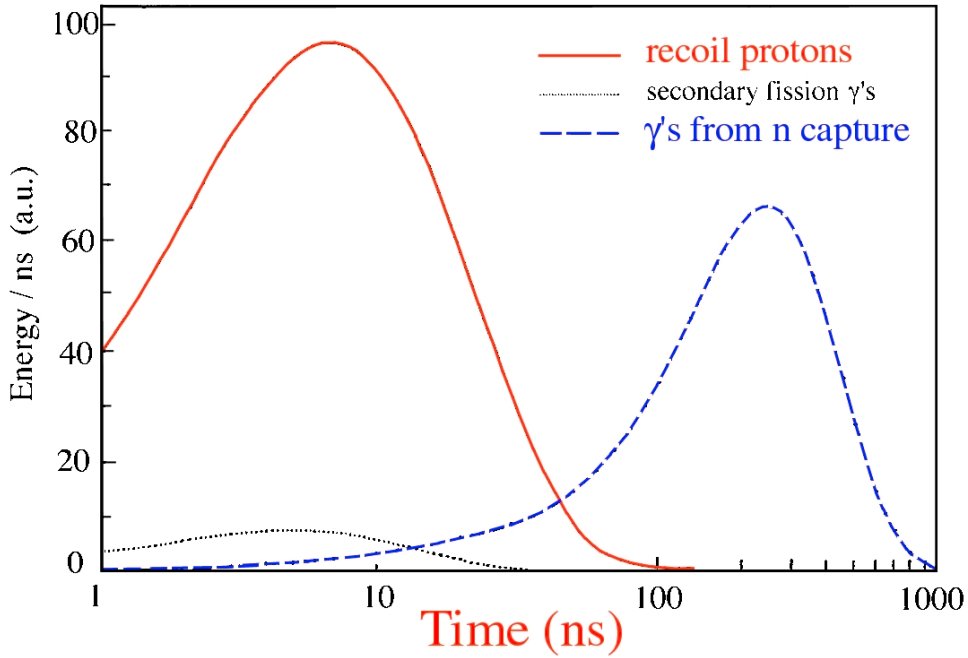

FIG. 3.22. Time structure of various contributions from neutron-induced processes to the hadronic signals of the ZEUS uranium/plastic-scintillator calorimeter [Bru 88].

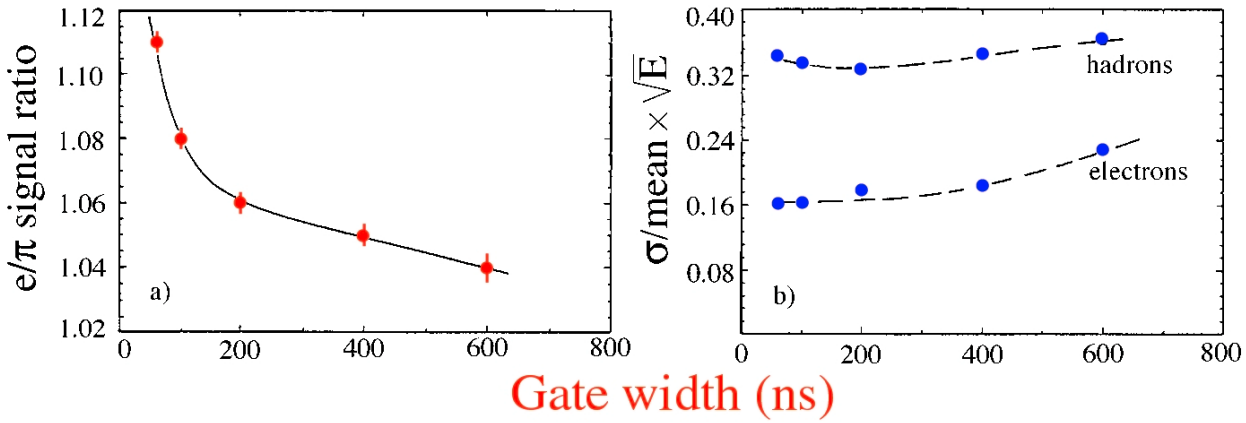

FIG. 3.23. The ratio of the average ZEUS calorimeter signals from 5 GeV/c electrons and pions (a) and the energy resolutions for detecting these particles (b), as a function of the charge integration time [Kru 92].

Compensation (4)

All compensating calorimeters rely on the contribution of *neutrons* to the signals

- *Ingredients* for compensating calorimeters:
  - *Sampling* calorimeter
  - *Hydrogenous* active medium (recoil p!)
  - Precisely tuned *sampling fraction*
    e.g. 10% for U/scintillator, 3% for Pb/scintillator,.....

- *Uranium* absorber

  Helpful, but neither *essential* nor *sufficient*

Fluctuations

- Calorimeter's energy resolution is determined by *fluctuations*
  → applying overall weighting factors (*"offline compensation"*) has **no merit** in this context

- Many sources of fluctuations may play a role, for example:
  - Signal quantum fluctuations (*e.g.*, photoelectron statistics)
  - Sampling fluctuations
  - Shower leakage
  - Instrumental effects (*e.g.*, electronic noise, light attenuation, structural non-uniformity)

  but usually one source dominates.

  Improve performance → work on that source

- Poissonian fluctuations:

  Energy E gives N signal quanta, with $\sigma = \sqrt{N}$

  $\rightarrow \sigma\sqrt{E} \propto \sqrt{N}\sqrt{N} = cE$

  $$\rightarrow \quad \frac{\sigma}{E} = \frac{c}{\sqrt{E}}$$

What excellent energy resolution does for you

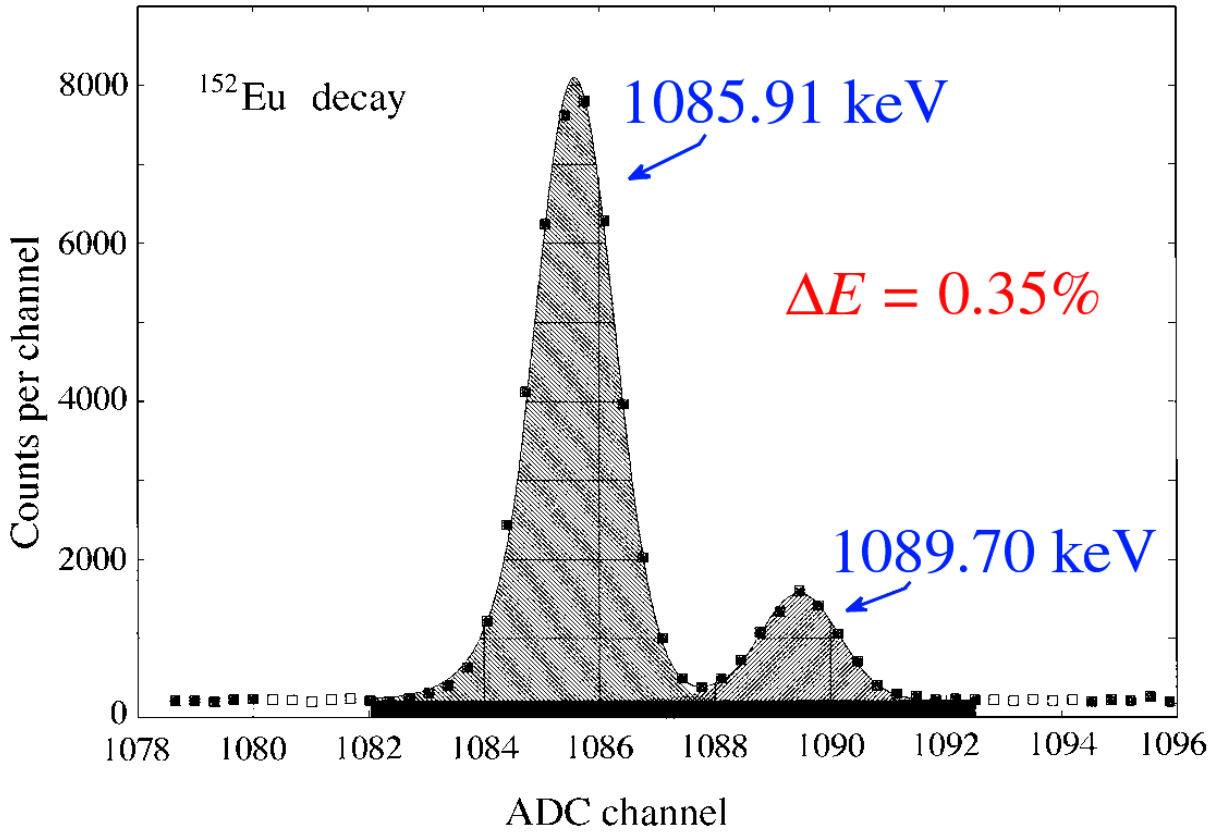

FIG. 4.1. Detection of nuclear γ-rays, from the decay of ^{152}Eu, with a high-purity germanium crystal. The energy resolution of this calorimeter is about 0.1% at 1 MeV. Courtesy of G. Roubaud, CERN.

Fluctuations (2)

- *Signal quantum fluctuations*
  - Ge detectors for nuclear γ ray spectroscopy: 1 eV/quantum
    $\rightarrow$ If $E = 1$ MeV: 10^6 quanta, therefore $\sigma/E = 0.1\%$
    Usually E expressed in GeV $\rightarrow \sigma/E = 0.003\%/\sqrt{E}$
  - Quartz fiber calorimeters: Typical light yield $\sim$ 1 photoelectron/GeV
    $\rightarrow \sigma/E = 100\%/\sqrt{E}$. If $E = 100$ GeV, $\sigma/E = 10\%$

Signal quantum fluctuations dominate (1)

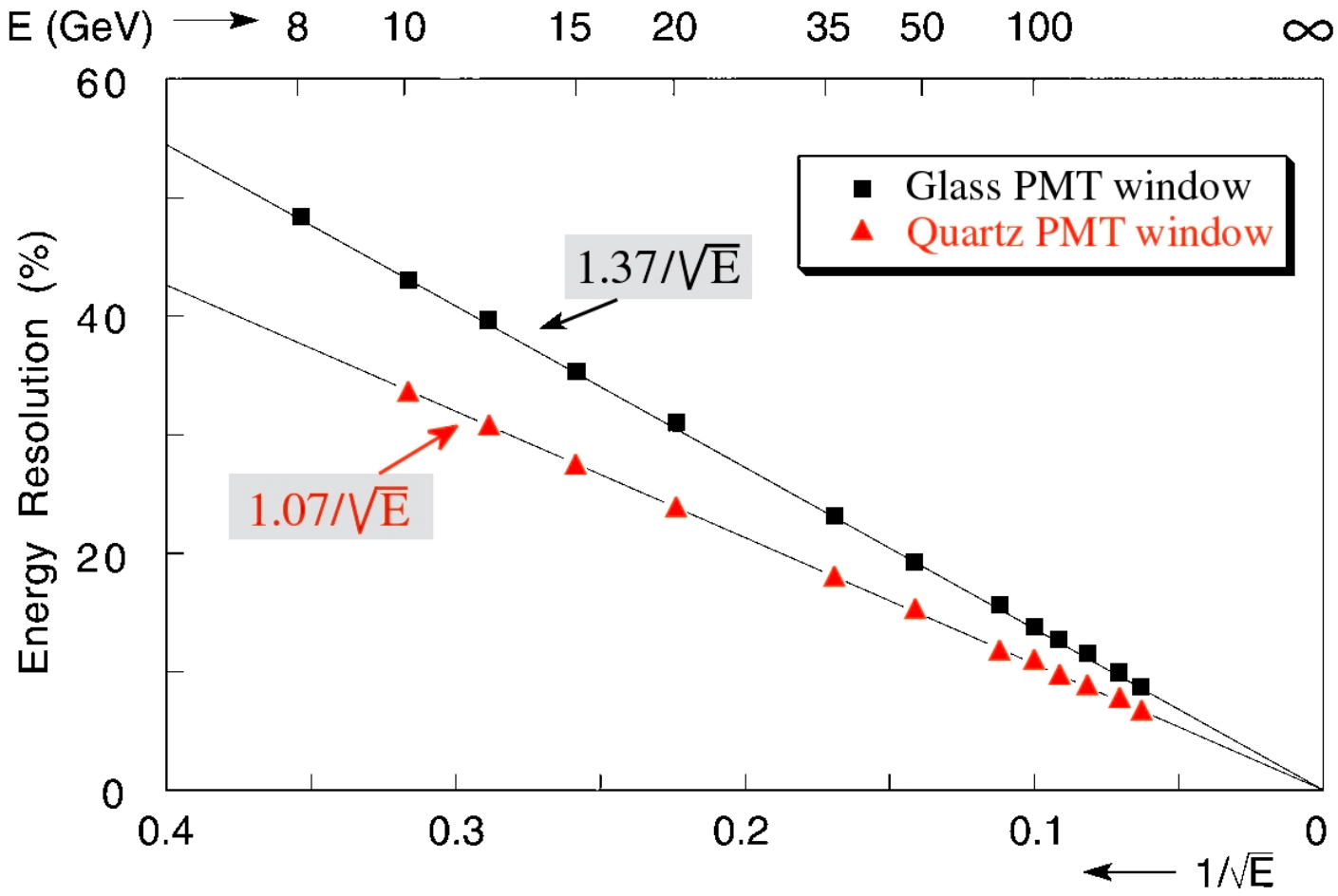

FIG. 4.2. The energy resolution for electron detection with the QFCAL prototype detector, as a function of energy. Results are given for measurements in which photomultiplier tubes with a glass window were used and for measurements in which the same type of PMTs were equipped with a quartz window [Akc 97].

Signal quantum fluctuations dominate also here (2)

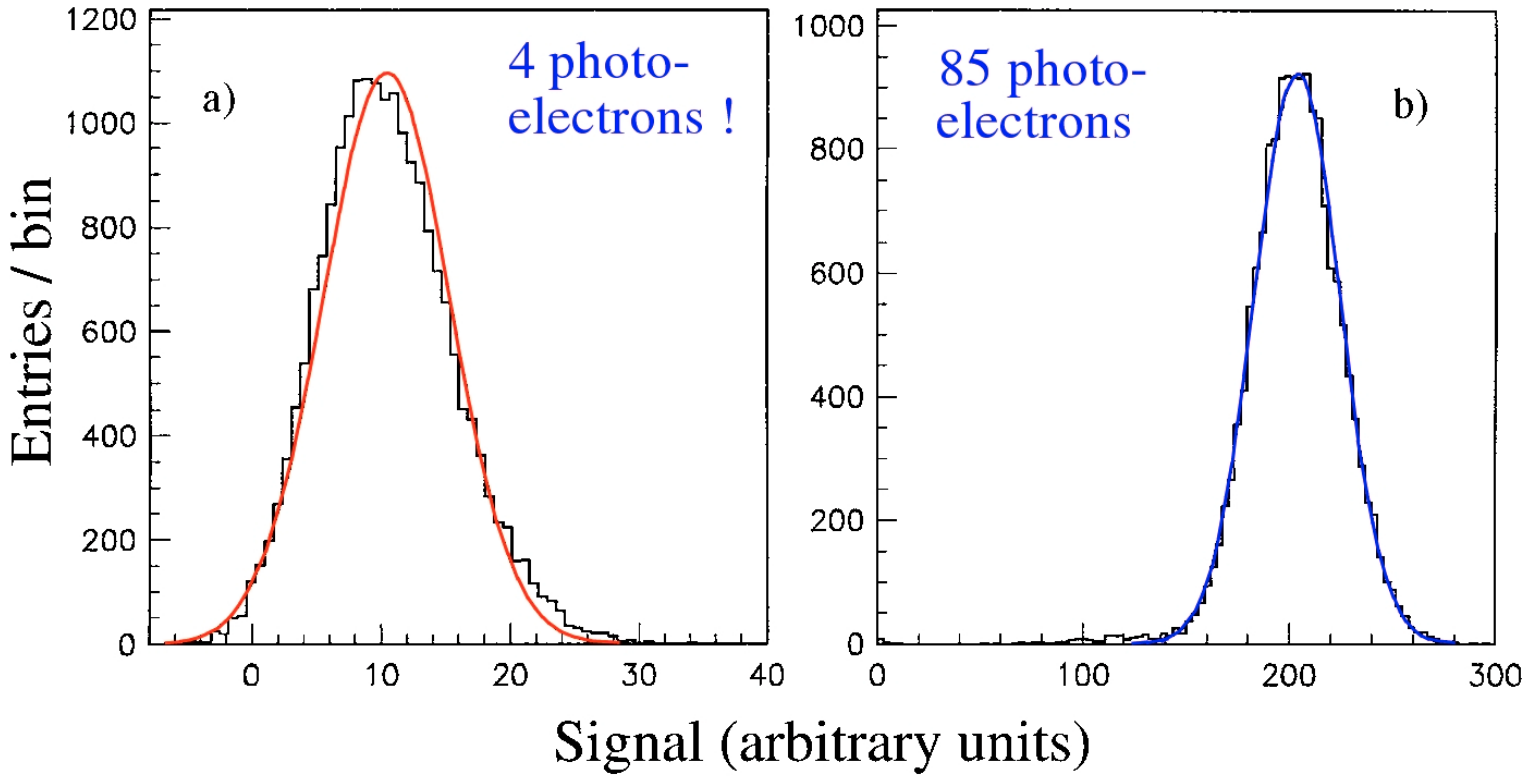

FIG. 4.3. Signal distributions for 10 GeV (a) and 200 GeV (b) electrons showering in the CMS Quartz-Fiber calorimeter, measured with a PMT with a glass window. The curves represent Gaussian fits to the experimental data [Akc 97].

Fluctuations (3)

- *Sampling fluctuations*

  Determined by fluctuations in the number of different shower particles contributing to the signals

  Both the sampling *fraction* and the sampling *frequency* are important

ZEUS: No correlation between particles contributing to signals in neighboring sampling layers $\rightarrow$ range of shower partcles is very small

Sampling fluctuations in em calorimeters
Determined by sampling fraction and sampling frequency

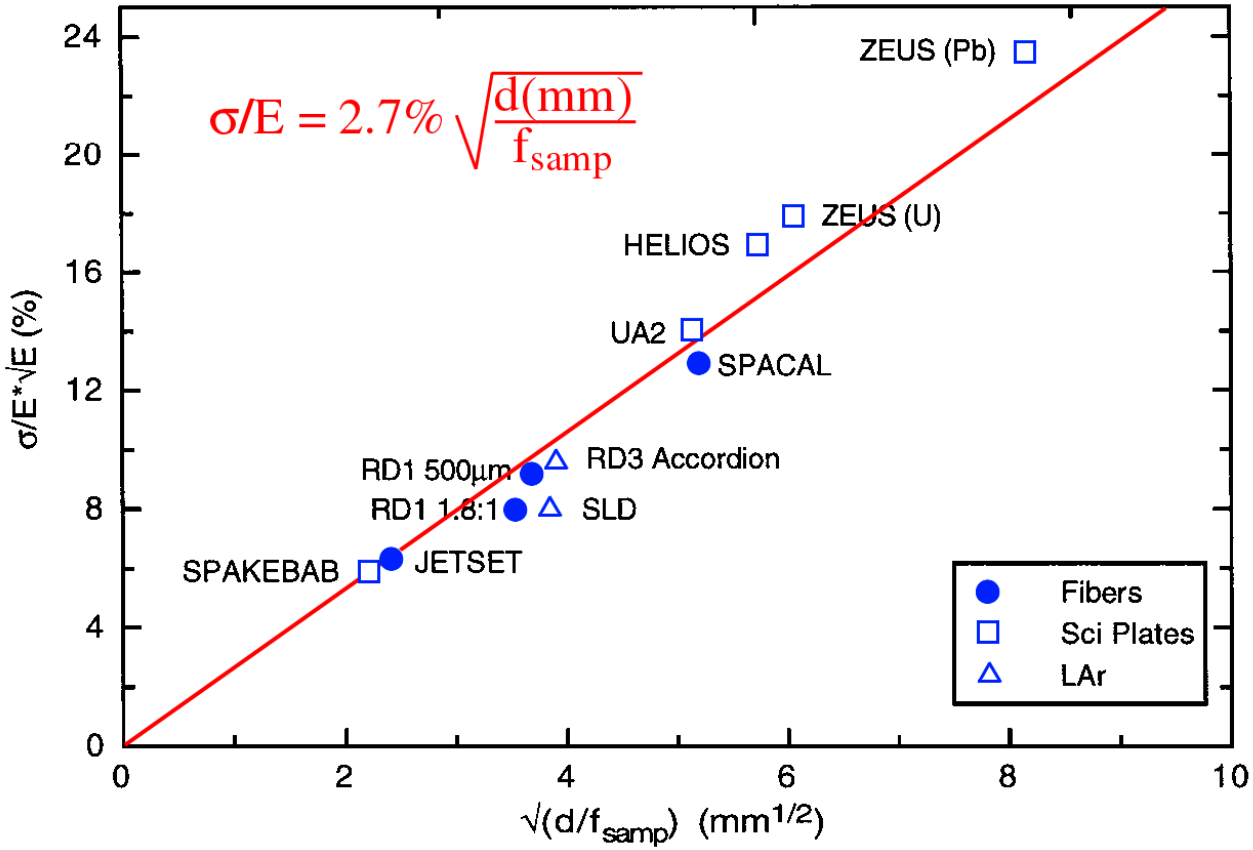

FIG. 4.8. The em energy resolution of sampling calorimeters as a function of the parameter $(d/f_{\rm samp})^{1/2}$, in which d is the thickness of an active sampling layer (*e.g.* the diameter of a fiber or the thickness of a scintillator plate or a liquid-argon gap), and $f_{\rm samp}$ is the sampling fraction for mips [Liv 95].

How to measure the effects of sampling fluctuations

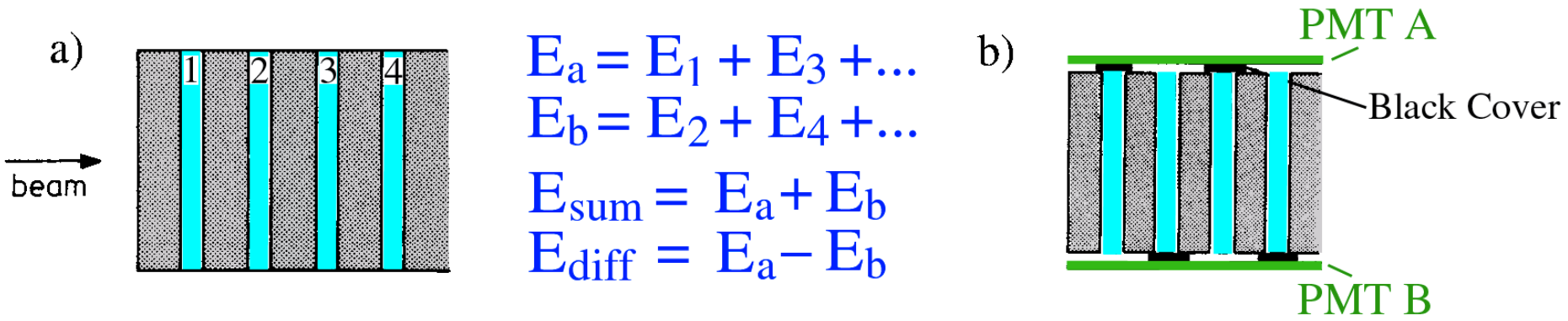

FIG. 4.13. Schematic structure of the ZEUS calorimeter (a) and the configuration used to measure the contribution of sampling fluctuations to the energy resolutions for em and hadronic showers (b).

Fluctuations (%)	*3 mm uranium* / *2.5 mm plastic* Electrons	Pions	*10 mm lead* / *2.5 mm plastic* Electrons	Pions
σ_A, σ_B	26.6±1.0	49.5±1.0	36.0±1.0	60.5±1.0
σ_{sum}	18.5±1.0	37.3±1.0	24.5±1.0	43.5±1.0
σ_{diff}	19.2±1.0	32.6±1.0	25.8±1.0	42.3±1.0
σ_{samp}	16.5±0.5	31.1±0.9	23.5±0.5	41.2±0.9
σ_{intr}	2.2±4.8	20.4±2.4	0.3±5.1	13.4±4.7

Table 4.1 *The contributions of sampling fluctuations and intrinsic fluctuations to the energy resolutions for electrons and pions in compensating uranium/plastic-scintillator and lead/plastic-scintillator calorimeters. Listed are the values of the coefficient a (Equation 4.1), expressed in %. Data from [Dre 90].*

How to measure the effects of sampling fluctuations (2)

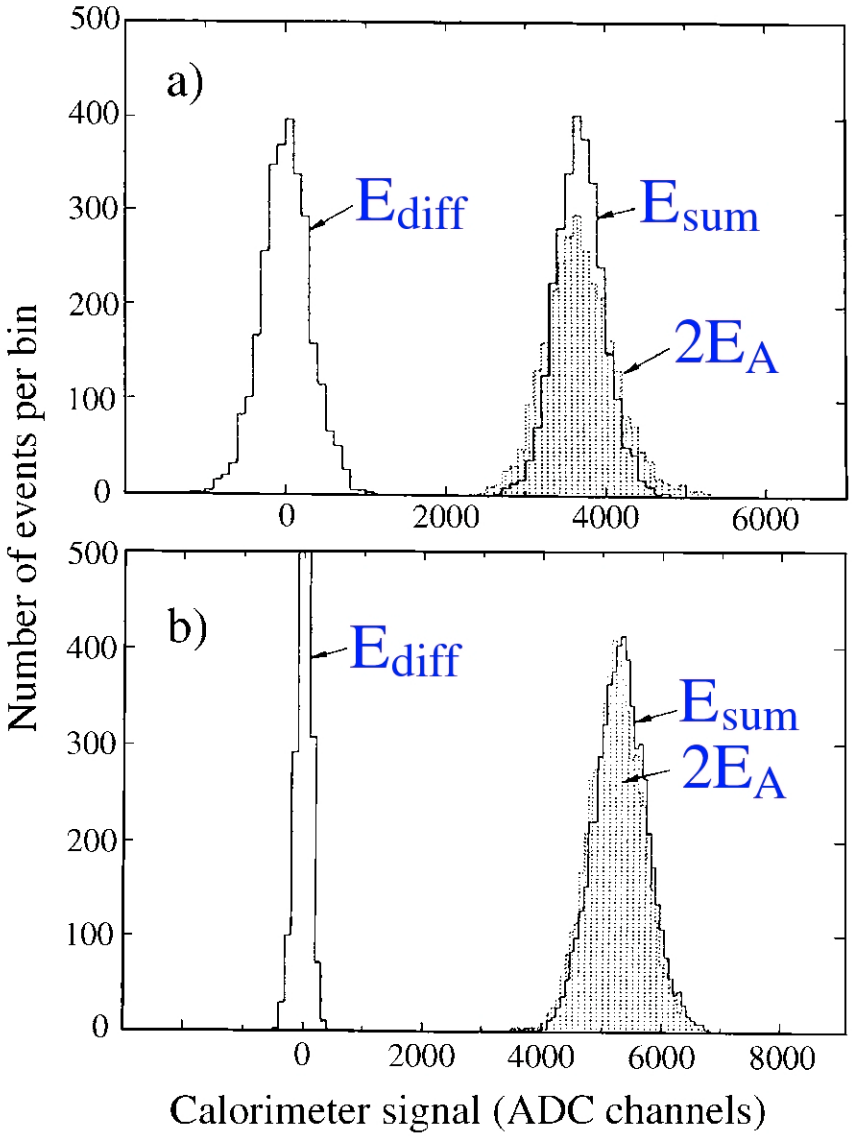

BLACK TAPE

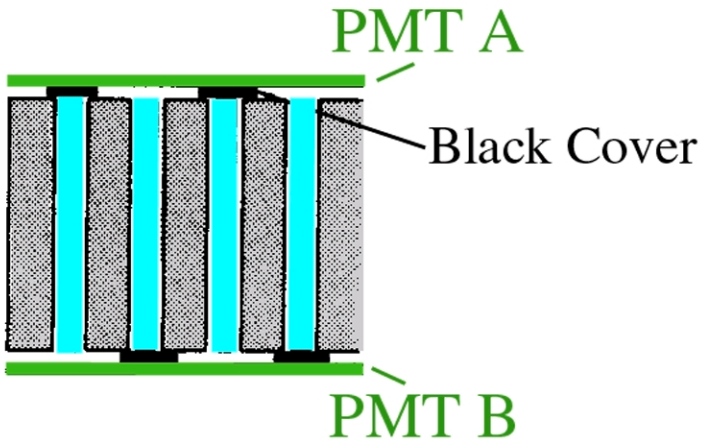

NO BLACK TAPE

FIG. 4.14. Pulse height distributions for 30 GeV hadrons obtained with the ZEUS lead/plastic-scintillator prototype calorimeter. Diagram a) shows the distributions of $E_{\rm sum}$, $E_{\rm diff}$ and $2E_{\rm A}$, measured in the configuration depicted in Figure 4.13b. Diagram b) shows the same distributions measured in the same configuration, but with the black tape removed. See text for details. From [Dre 90].

Sampling fluctuations in em and hadronic showers

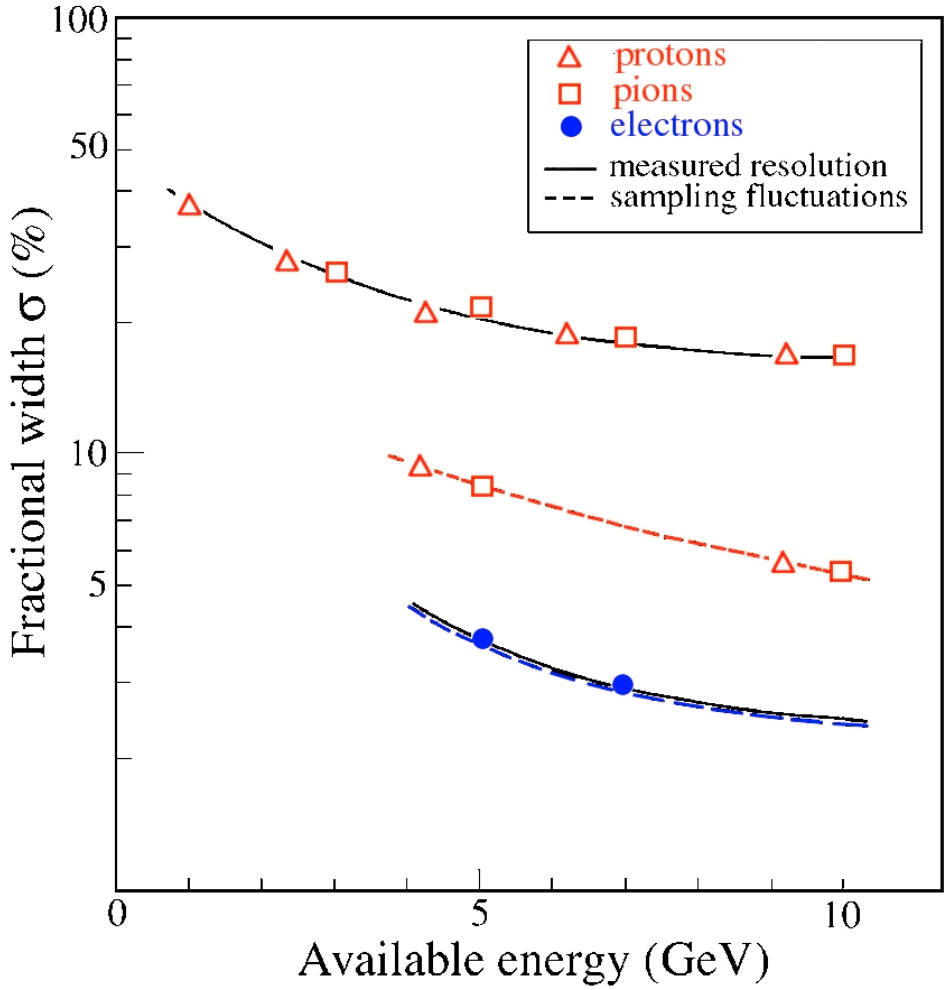

FIG. 4.15. The energy resolution and the contribution from sampling fluctuations to this resolution measured for electrons and hadrons, in a calorimeter consisting of 1.5 mm thick iron plates separated by 2 mm gaps filled with liquid argon. From [Fab 77].

Fluctuations (4)

- *Shower leakage fluctuations*
  - These fluctuations are *non-Poissonian*
  - For a given average containment, *longitudinal* fluctuations are *larger than lateral* ones.

    Difference comes from # of particles responsible for leakage.

    e.g. Differences between e, γ induced showers

Contribution of leakage fluctuations to energy resolution

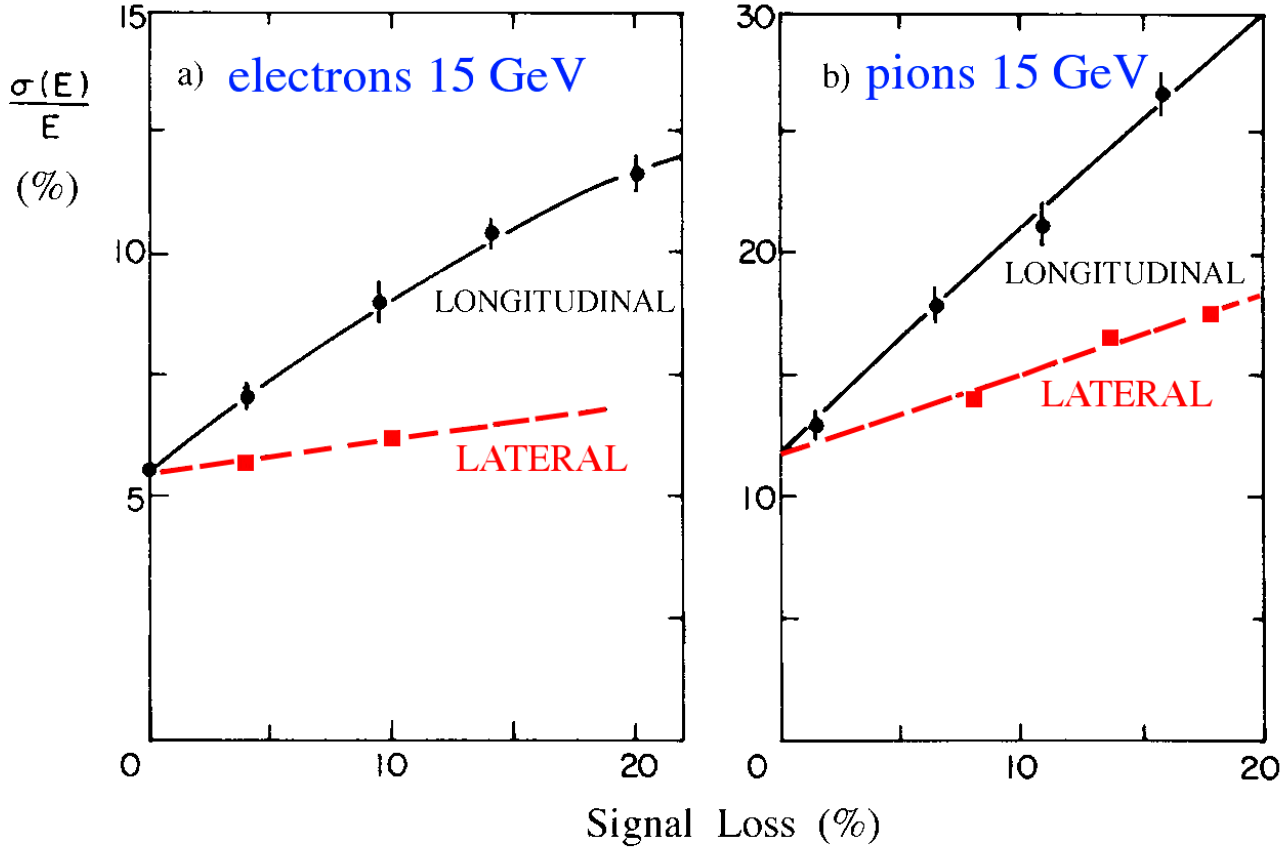

FIG. 4.28. The effects of longitudinal and lateral shower leakage on the energy resolution, as measured for 15 GeV electrons (a) and pions (b) by the CHARM Collaboration in a low-Z calorimeter [Did 80, Amal 81].

Effects back-, front-, and side leakage on em energy resolution

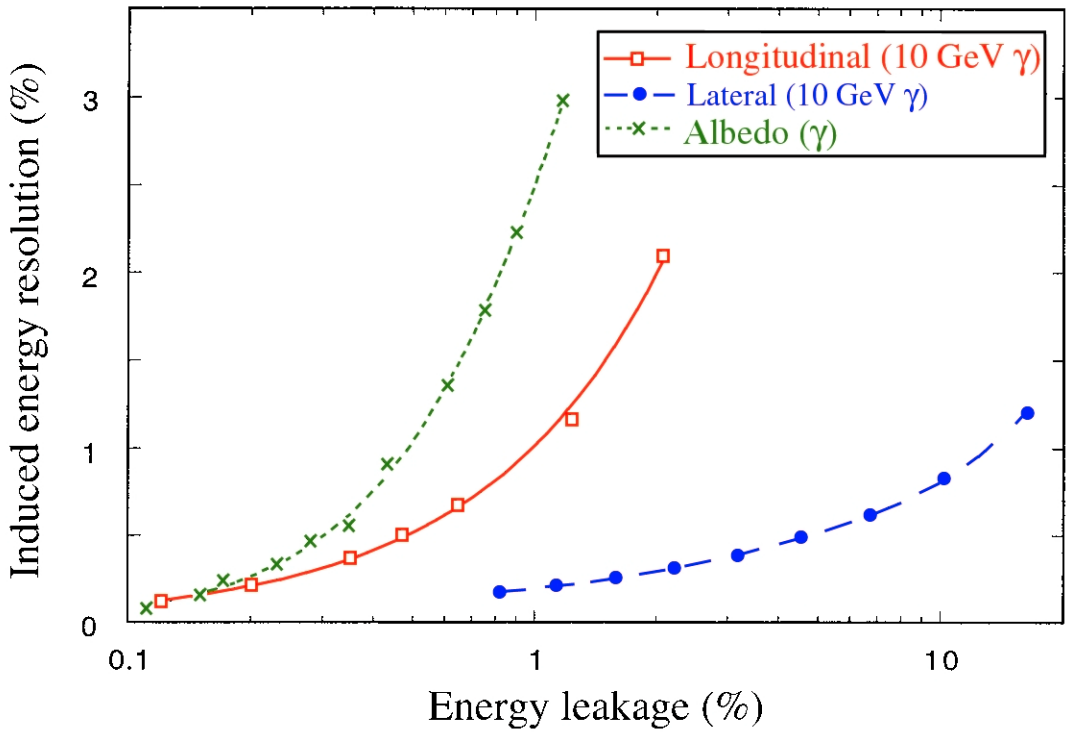

FIG. 4.37. A comparison of the effects caused by different types of shower leakage. Shown are the induced energy resolutions resulting from albedo, longitudinal and lateral leakage as a function of the average energy fraction carried by particles escaping from the detector. The longitudinal and lateral leakage data concern 10 GeV γs, the albedo data are for γ-induced showers of different energies. Results from EGS4 Monte Carlo calculations.

Leakage and leakage fluctuations in electron / γ induced showers

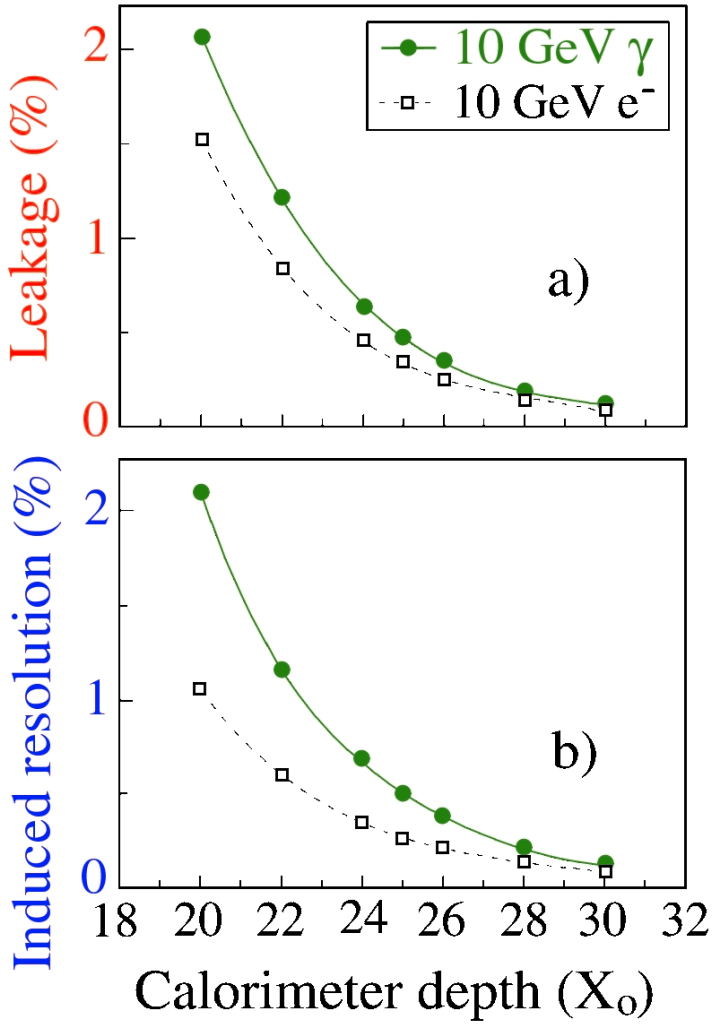

Figure 5: The average fraction of the shower energy carried by particles escaping the calorimeter through the back plane (a) and the relative increase in the energy resolution caused by this effect (b), for showers induced by 10 GeV electrons and 10 GeV γs developing in blocks of tin with different thicknesses, ranging from $20X_0$ to $30X_0$. Results from EGS4 Monte Carlo calculations.

Fluctuations (5)

- *Instrumental effects*
  - Structural differences in sampling fraction
  - "Channeling" effects
  - Electronic noise, light attenuation,.....

Instrumental effects: Channeling in fiber calorimeters

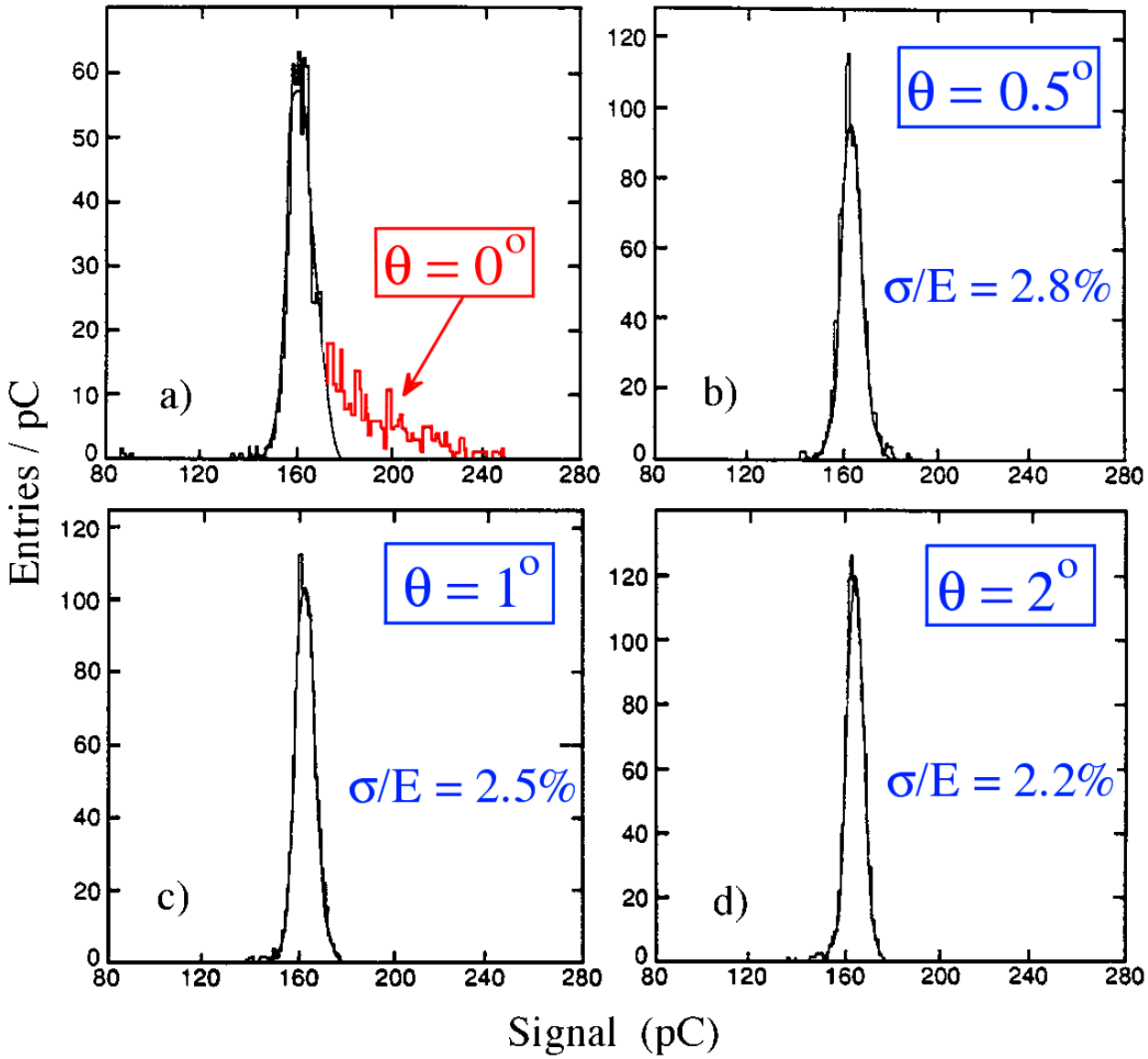

FIG. 4.22. Signal distributions for 40 GeV electron showers measured with the RD1 0.5 mm fiber calorimeter, for different angles between the particle s direction and the fiber [Bad 94a].

Fluctuations (6)

- Different effects have *different energy dependence*

quantum, sampling fluctuations:	$\sigma/E \sim E^{-1/2}$
shower leakage	$\sigma/E \sim E^{-1/4}$
electronic noise	$\sigma/E \sim E^{-1}$
structural non-uniformities	σ/E = constant

Add in quadrature: $\sigma_{tot}^2 = \sigma_1^2 + \sigma_2^2 + \sigma_3^2 + \sigma_4^2 ...$

The em energy resolution of the ATLAS calorimeter

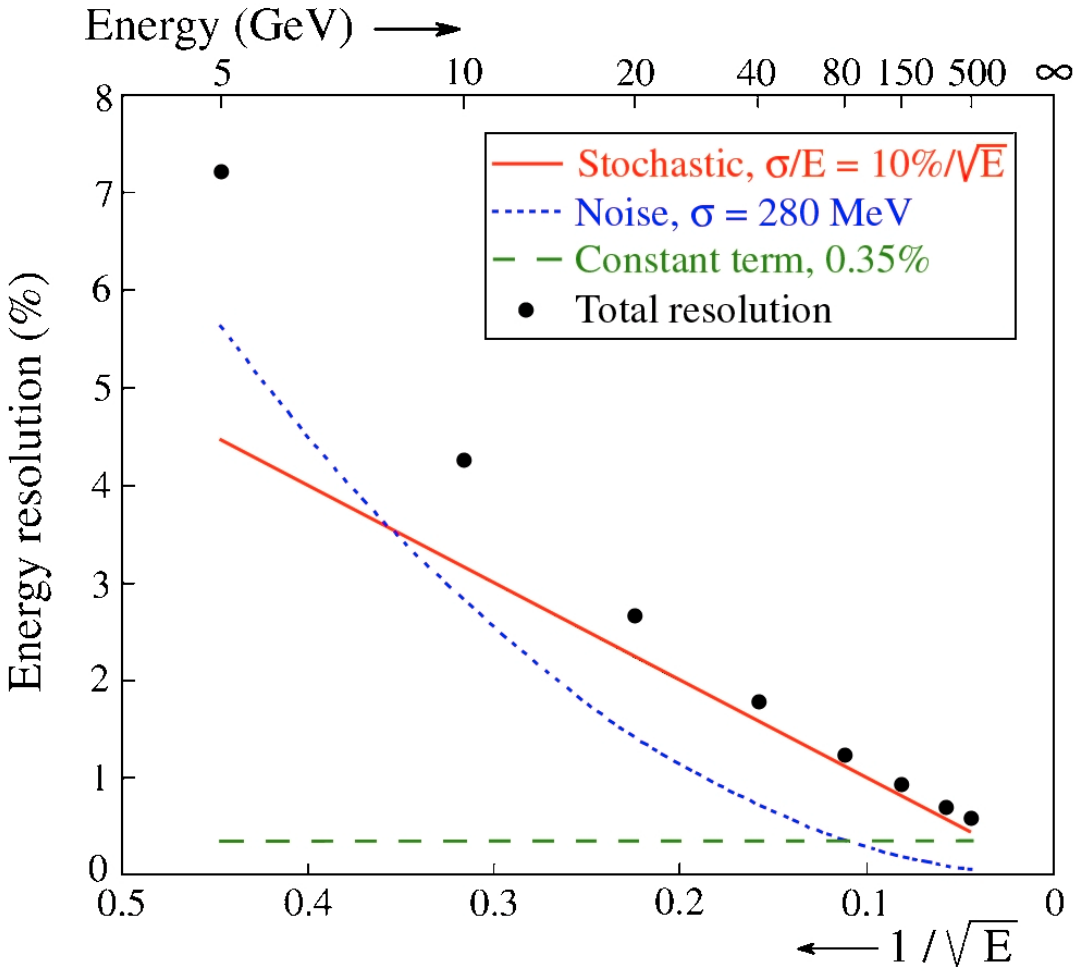

FIG. 9.30. The em energy resolution and the separate contributions to it, for the em barrel calorimeter, at $\eta = 0.28$ [Gin 95].

Fluctuations in Hadron Showers

Same types of fluctuations as in em showers, *plus*

- Fluctuations in *visible energy*
  (ultimate limit of hadronic energy resolution)

- Fluctuations in the *em shower fraction*, f_{em}
  - *Dominating effect* in most hadron calorimeters ($e/h \neq 1$)
  - Fluctuations are *asymmetric* in pion showers (one-way street)
  - *Differences* between p, π induced showers
    No leading π^0 in proton showers (baryon # conservation)

Hadron showers: Fluctuations in nuclear binding energy losses

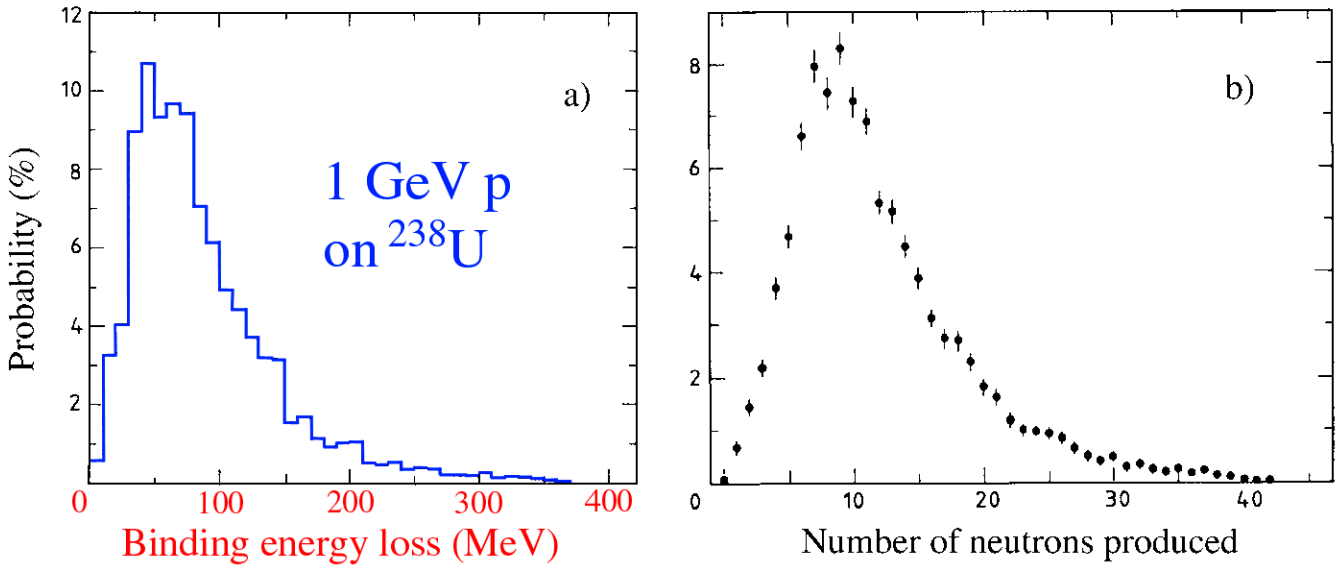

FIG. 4.43. The nuclear binding energy lost in spallation reactions induced by 1 GeV protons on ^{238}U nuclei (a), and the number of neutrons produced in such reactions (b). From [Wig 87].

Fluctuations in Hadron Showers

Same types of fluctuations as in em showers, *plus*

- Fluctuations in *visible energy*
  (ultimate limit of hadronic energy resolution)

- Fluctuations in the *em shower fraction*, f_{em}
  - *Dominating effect* in most hadron calorimeters ($e/h \neq 1$)
  - Fluctuations are *asymmetric* in pion showers (one-way street)
  - *Differences* between p, π induced showers
    No leading π^0 in proton showers (baryon # conservation)

Hadron showers: Fluctuations in em shower fraction (f_{em})

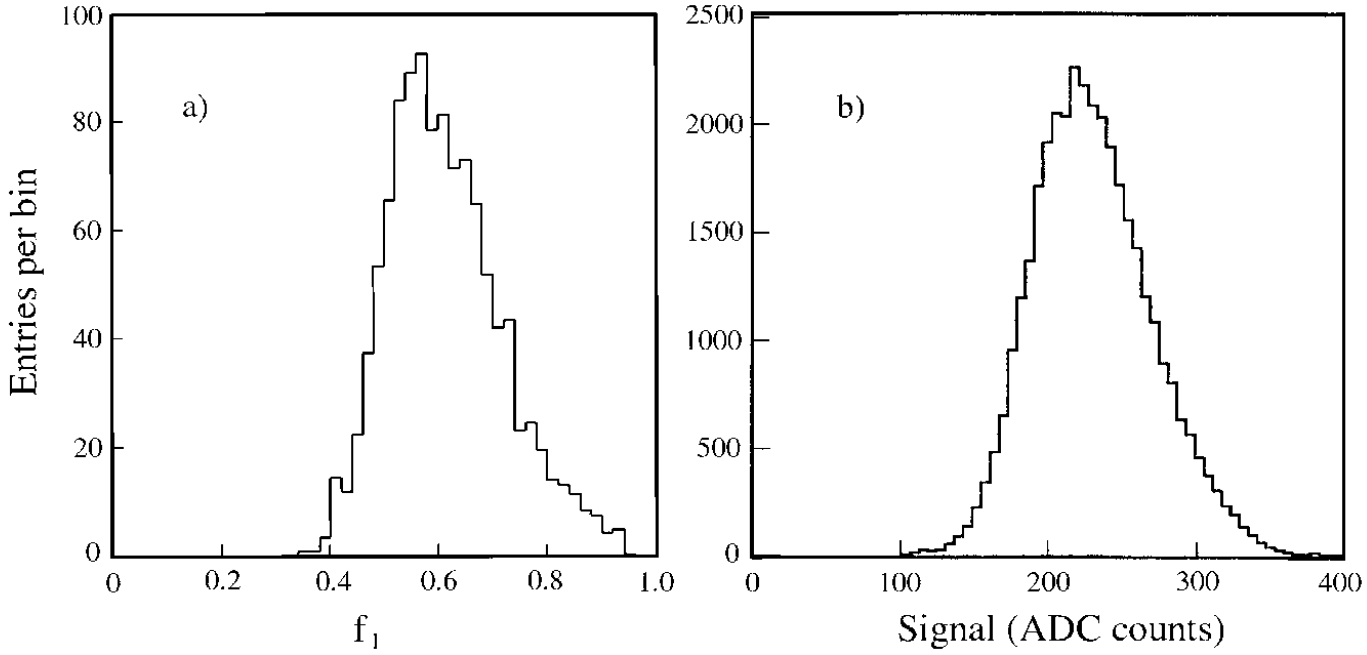

FIG. 4.44. The distribution of the fraction of the energy of 150 GeV π^- showers contained in the em shower core, as measured with the SPACAL detector (a) [Aco 92b] and the signal distribution for 300 GeV π^- showers in the CMS Quartz-Fiber calorimeter (b) [Akc 98].

Hadronic response function: Effect of e/h

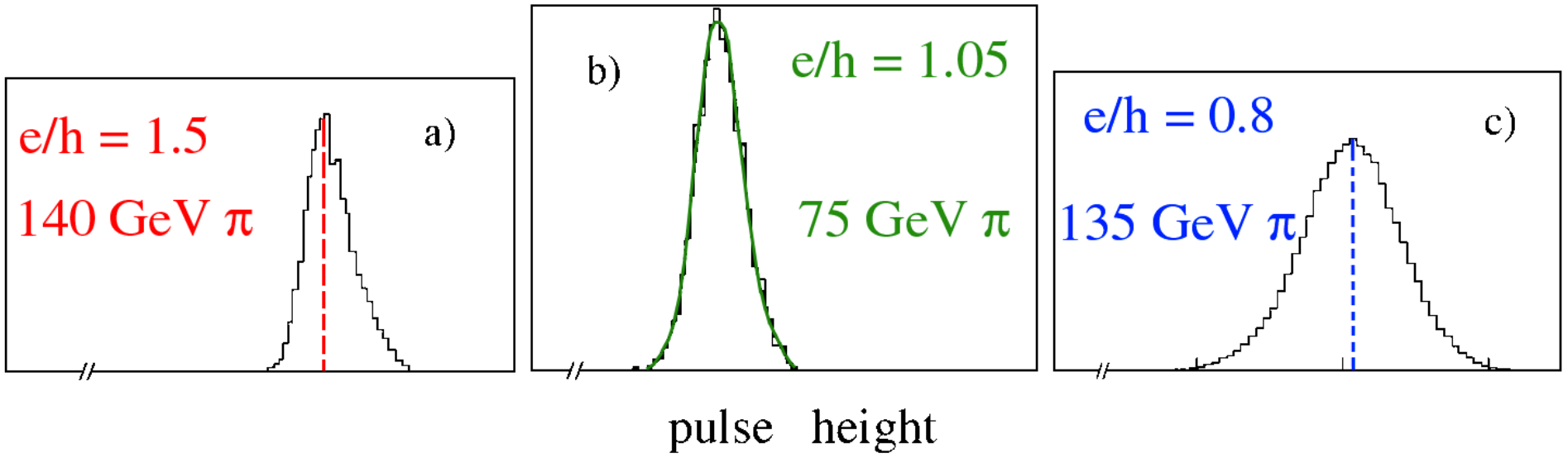

FIG. 7.24. Signal distributions for mono-energetic pions in calorimeters with different e/h values. Data from WA1 [Abr 81], ZEUS [Beh 90] and WA78 [Dev 86].

Fluctuations in f_{em}: Differences p/π induced showers

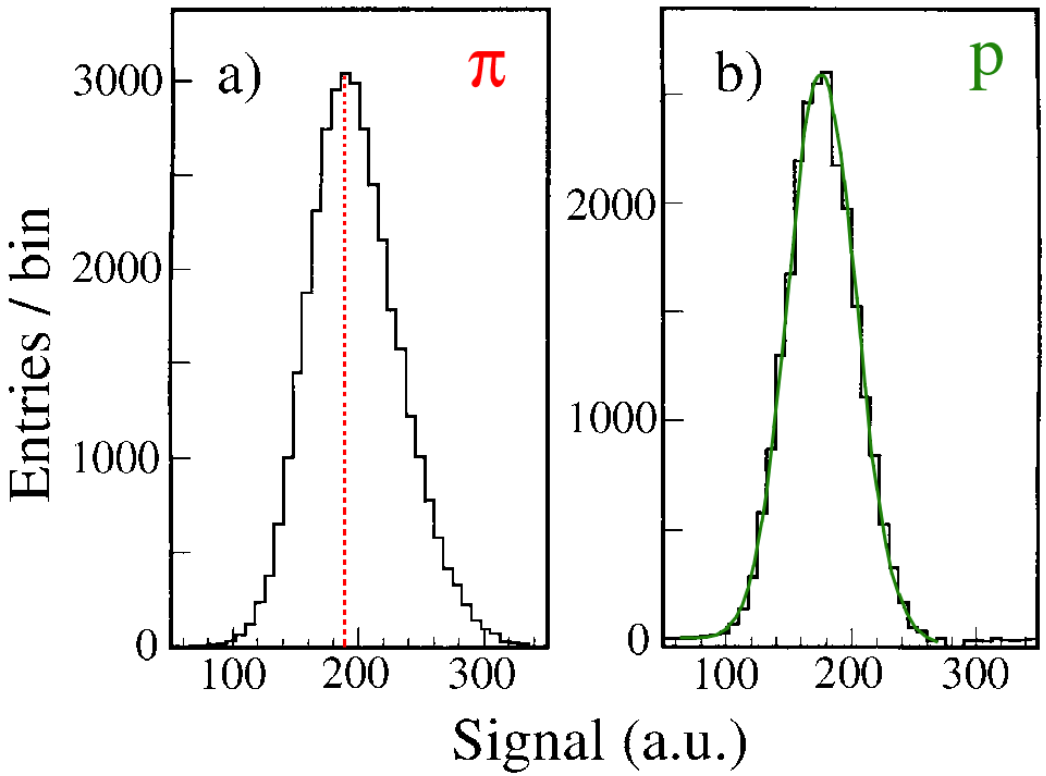

FIG. 4.49. Signal distributions for 300 GeV pions (a) and protons (b) detected with a quartz-fiber calorimeter. The curve represents the result of a Gaussian fit to the proton distribution [Akc 98].

Fluctuations in Hadron Showers (2)

- Effect of non-compensation on σ/E is *not* a constant term

In practice, $\boxed{\frac{\sigma}{E} = \frac{a}{\sqrt{E}} + b}$ is a good approximation

Hadronic resolution of non-compensating calorimeters

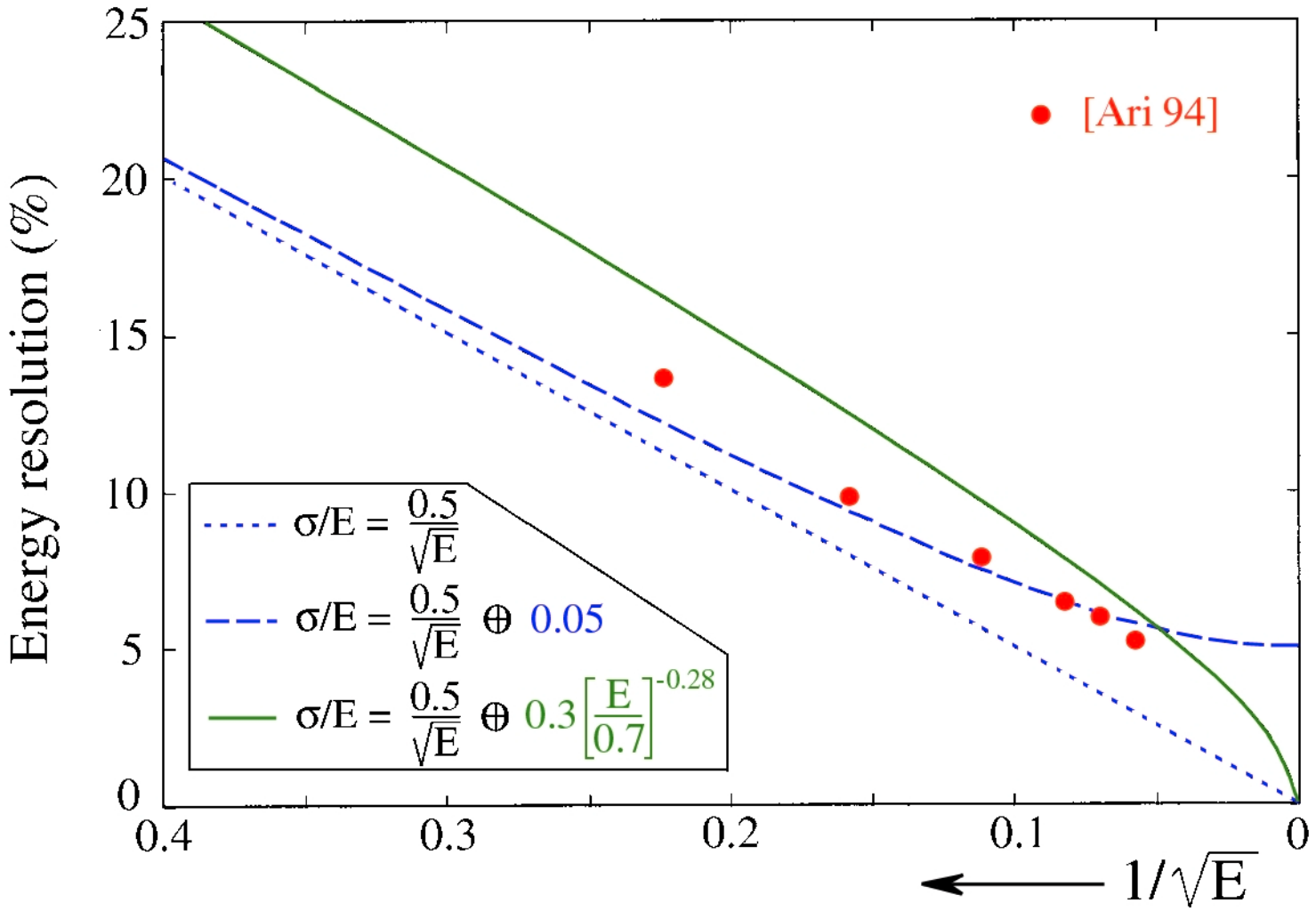

FIG. 4.47. Comparison between Equations 4.28 (the dashed curve) and 4.29 (the solid curve). The dotted line represents the stochastic term in these equations. The experimental data were taken from [Ari 94]. See text for details.

Hadronic resolution of non-compensating calorimeters

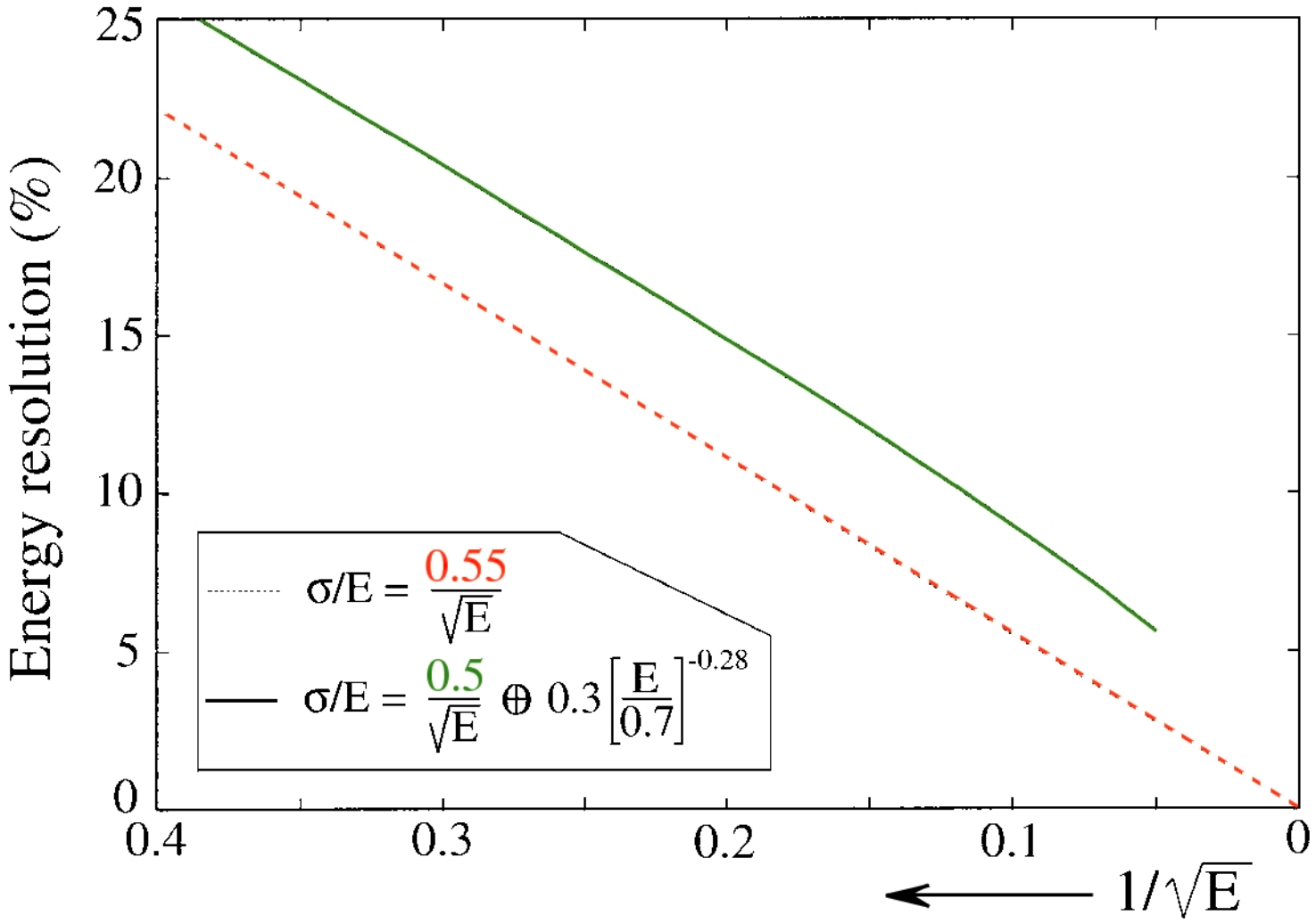

FIG. 4.48. The energy resolution calculated with Equation 4.29 for energies up to 400 GeV (the solid line), and calculated with a sole stochastic term with a slightly larger a_1 value (the dotted line). See text for details.

Fluctuations in Hadron Showers (3)

- The *ultimate limit* on hadronic energy resolution is determined by the correlation between ΣE_n and nuclear binding energy loss

  Better in Pb than in Uranium ($13\%/\sqrt{E}$ *vs.* $20\%/\sqrt{E}$)

The ultimate limit on hadronic energy resolution

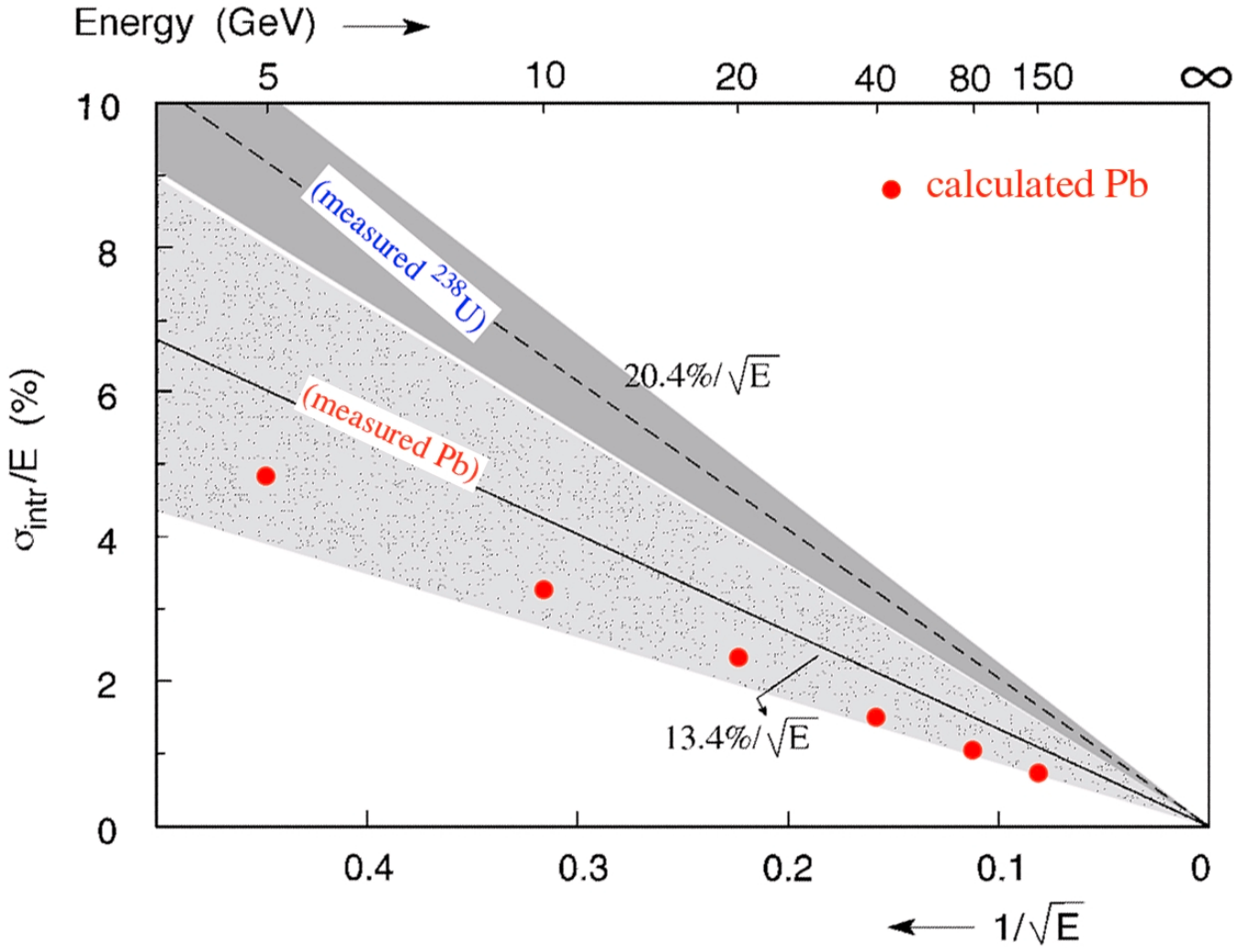

FIG. 4.55. The (calculated) contribution of fluctuations in the total kinetic energy carried by neutrons to the hadronic energy resolution of a compensating Pb/plastic-scintillator calorimeter, as a function of energy (the black dots). The measured value of the irreducible fluctuations in such a calorimeter is indicated by the shaded area. The dashed line represents the measured value of the irreducible fluctuations in a compensating ^{238}U/plastic-scintillator calorimeter.

Lessons for calorimeter design (1)

- *Improve* resolution → work on fluctuations that *dominate*

  Example: 60 ton **(liquid)** scintillator does not make good hadron calorimeter
  All fluctuations eliminated, except non-compensation: $\sigma/E > 10\%$ at all energies!

  SPACAL ($e/h \approx 1.0$, but other sources of fluctuation present):
  $\sigma/E \approx 2\%$ at $E = 300$ GeV

Hadron calorimeters: Effects f_{em} fluctuations on resolution

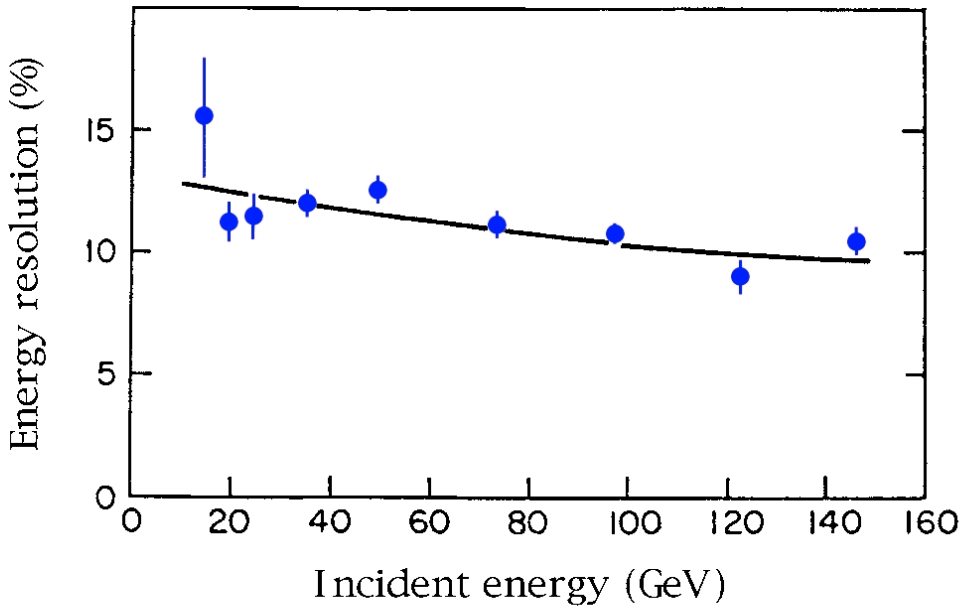

Figure 9: The hadronic energy resolution as a function of energy, for a homogeneous calorimeter consisting of 60 *tonnes of liquid scintillator*

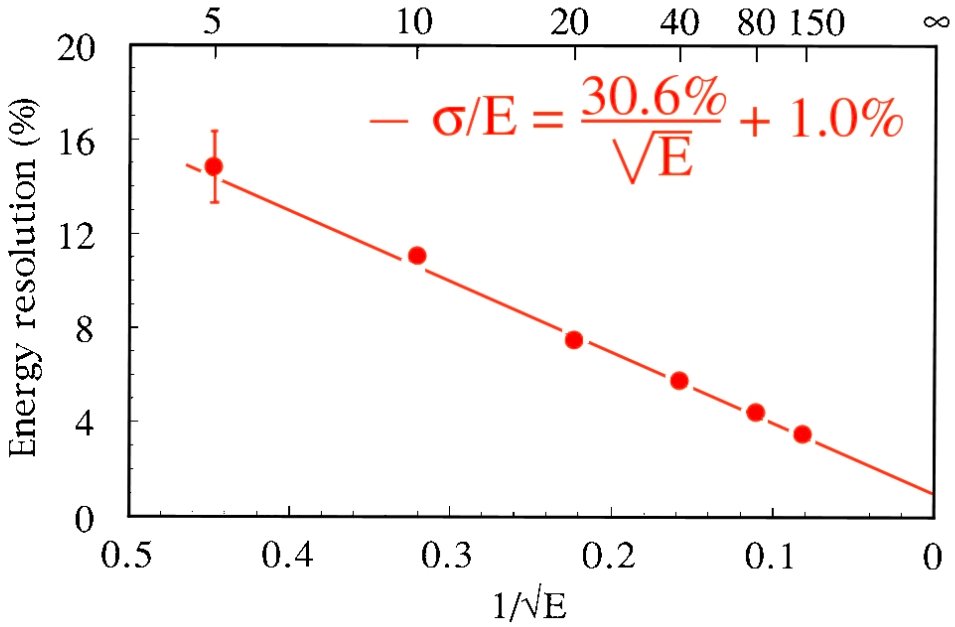

Figure 10: The hadronic energy resolution as a function of energy, for the compensating SPACAL *lead/plastic-scintillator calorimeter (sampling fraction 2%)*

Lessons for calorimeter design (2)

- Do not spend your money reducing fluctuations that do *not* dominate

Practical examples:

- A $2\lambda_{\rm int}$ deep calorimeter for extraterrestrial detection of high energy cosmic hadrons is dominated by *shower leakage*

➡ A high-quality crystal calorimeter is as good (bad) as a crudely sampling one

- A calorimeter system with a crystal em section will have poor performance for hadron detection, *no matter what* you choose as the hadronic section, because of the large e/h value of homogeneous devices

➡ *Don't waste your money on the hadronic section*

Dominating fluctuations dominate

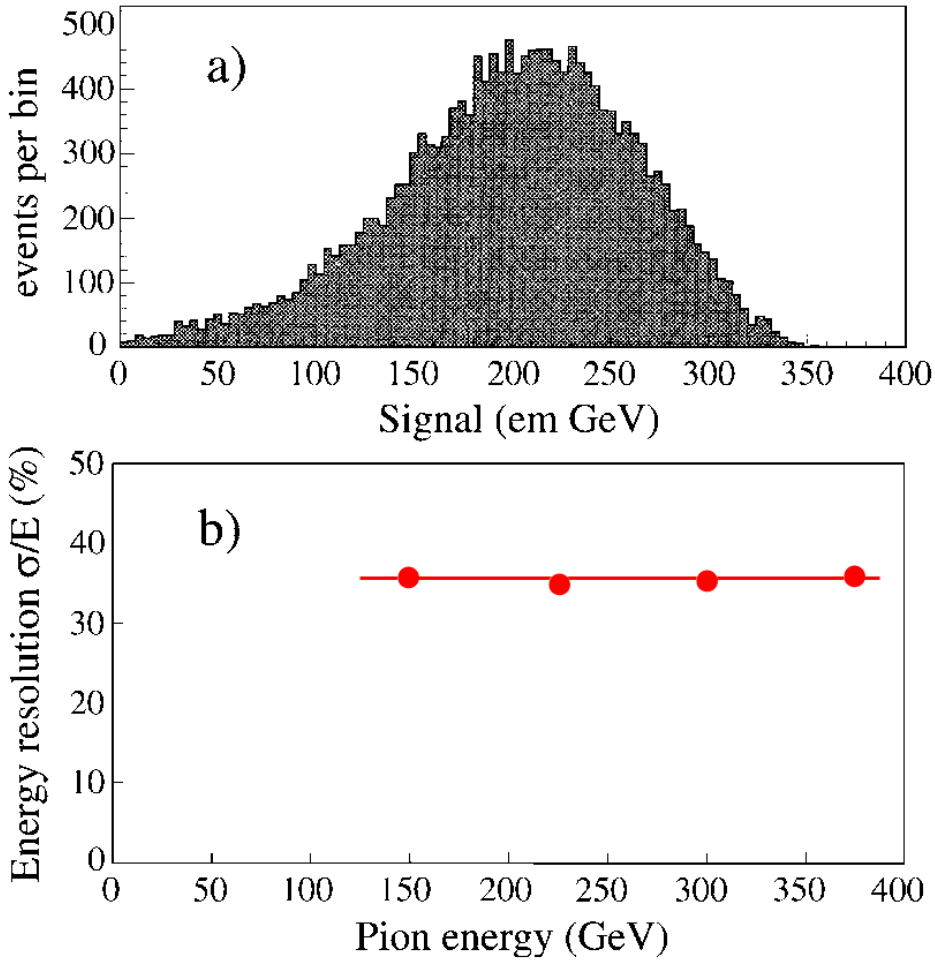

Figure 4: *Signal distribution for 375 GeV π^- in a $1.4\lambda_{\text{int}}$ deep calorimeter (a) and the energy resolution of this detector as a function of the pion energy (b).*